Reconstruction of anthropogenic activities in legacy sediments from the Eure River, a major tributary of the Seine Estuary (France)

Thomas Gardes, Maxime Debret, Yoann Copard, Edouard Patault, Thierry Winiarski, Anne-Lise Develle, Pierre Sabatier, André-Marie Dendievel, Brice Mourier, Stéphane Marcotte, et al.

Reconstruction of anthropogenic activities in legacy sediments from the Eure River, a major tributary of the Seine Estuary (France)

Thomas Gardes[1,2,*], Maxime Debret[1], Yoann Copard[1], Edouard Patault[1], Thierry Winiarski[3], Anne-Lise Develle[4], Pierre Sabatier[4], André-Marie Dendievel[3], Brice Mourier[3], Stéphane Marcotte[5], Barbara Leroy[6], Florence Portet-Koltalo[2]

[1]Normandie Univ, Rouen, UNIROUEN, UNICAEN, CNRS, M2C, 76000 Rouen, France.

[2]Normandie Univ, Rouen, UMR CNRS 6014 COBRA, 55 Rue Saint Germain, 27000 Evreux, France.

[3]Université Lyon 1, ENTPE, UMR CNRS 5023 LEHNA, 3 Rue Maurice Audin, 69518 Vaux-en-Velin, France.

[4]Université Grenoble Alpes, Université Savoie Mont Blanc, CNRS, EDYTEM, 73000 Chambéry, France.

[5]Normandie Univ, Rouen, INSA de Rouen, UMR CNRS 6014 COBRA, Avenue de l'Université, 76801 Saint-Etienne-du-Rouvray Cedex, France.

[6]Agence de l'eau Seine-Normandie, Quai de Boisguilbert, 76000 Rouen, France.

[*]Corresponding author: thomas.gardes2@univ-rouen.fr

Keywords: Anthropogenic Activities, Eure River, Legacy Sediments, Sediment Cores, Trace Metals.

Abstract

Most rivers worldwide are contaminated by various trace metals from different origins, which may be stored for considerable periods of time in depositional areas. Most of these studies are focused on the main river of a watershed and the tributaries are often neglected which can be important sources of contamination. The aim of this study was to reconstruct the anthropogenic activities that occurred in the Eure River, tributary of the Seine Estuary, since the 1940s using "legacy sediments". The results showed that the temporal trends of trace metals were not related to detrital inputs and TOC variations but with the industrial history of the Eure River watershed. The high levels of Zn, Cu, and Ni during the 1950s and the 1960s and the decrease with the decline of the probable main source of release showed the watershed reactivity to anthropogenic activities. The high levels of Pb during the 1990s and the 2000s showed that the watershed reacted immediately to anthropogenic pressures. The Pb levels remained important after the cease of industrial activity, showing that a resilience period is necessary for the system, and that interactions between human activities and the environment go beyond of the activities themselves.

1. Introduction

Many researchers agree that the Earth has entered a new geological period, the Anthropocene (Crutzen and Stoermer, 2000; Crutzen, 2006; Steffen et al., 2011; Lewis and Maslin, 2015). While the beginning of this period is the subject of intense debate (Lewis and Maslin, 2015), there is consensus that humans have seriously impacted their environment during this period (Steffen et al., 2011). Such human activities as agriculture, forestry, mining,

and water storage and diversion contribute significantly to landscape change and environmental contamination. The sediments generated by the erosive actions of humans have received increasing attention in recent years and have even been categorised as a particular type, known as legacy sediments (James, 2013, 2018); these are generally defined as alluvial sediments that are deposited as a result of anthropogenic disturbances within a watershed (James, 2013). Among the several sedimentation and storage zones throughout the watershed, there is particular concern about how legacy sediments trapped behind dams are managed (i.e. dredging). Structures such as dams change the flow of a river to achieve particular objectives (e.g. energy production, flood control, and navigation) and serve to modify the hydrodynamic cycle and thus the sediment storage in catchment (Nilsson et al., 2005; Yang et al., 2006). Many studies have examined the storage of metallic and organic contaminants behind dams (e.g. Shuman, 1995; Müller et al., 2000; Bednarek, 2001; Stanley and Doyle, 2003; Audry et al., 2004; Ashley et al., 2006; Devault et al., 2009; Dhivert et al., 2015; Evans, 2015). Hence, legacy sediments can be viewed as the industrial and agricultural testimonies of past anthropogenic activities in, and can reflect the trajectory of, any studied watersheds. In addition, estuaries are dynamic environments where it is difficult to reconstruct temporal trends of contamination and the origins of these latter from legacy sediments. So, determining the origins of contamination in an estuary requires to study its tributaries.

The Seine River watershed (France) provides an example of a basin experiencing anthropogenic activities. The industrial revolution increased the anthropogenic pressure on the Seine River considerably over a period of about 150 years, resulting in specific and drastic changes in the stream morphology. These modifications meant that the flow of the Seine River was regulated, mainly to facilitate navigation in the nineteenth century (Horowitz et al., 1999; Lestel et al., 2019). The morphological modifications also impacted the tributaries of the Seine River. Thus, the Eure River, the most important contributor to the Seine Estuary, saw its outlet diverted 11 km downstream between 1929 and 1939. All these adjustments have

promoted the establishment of depositional environments favouring the storage of legacy sediments suitable for reconstructing anthropogenic activities in the watershed. However, if the history of the Seine River is well known, there is less historical information about its tributaries; the latter could potentially be the main source of contamination in the lower reaches of the watershed, i.e., the estuary (e.g. the Gironde Estuary; Audry et al., 2004; Masson et al., 2006). Most sediment cores covering at least the last 70 years were extracted along the Seine Estuary (Van Metre et al., 2008; Vrel, 2012; Vrel et al., 2013; Kaci et al., 2014, 2016) and along the fluvial part of the Seine River, upstream from the Poses Dam (Figure 1A; Bonté et al., 2004; Meybeck et al., 2007; Ayrault et al., 2010a; Le Cloarec et al., 2011; Tamtam et al., 2011; Ayrault et al., 2012; Vrel et al., 2013; Lorgeoux et al., 2016). In contrast, there are few sediment records for the tributaries (Figure 1B; Ayrault et al., 2010b; Le Cloarec et al., 2011; Ayrault et al., 2012). Unfortunately, the geographic locations of the cores from the Oise and Marne rivers restricted the reconstruction of the sedimentary and contamination history to a limited area of these two tributaries. The best location for coring is at the outlet of a tributary, where the geochemical signatures of the river being studied can best be captured.

This is the reason that anthropogenic activities in the Eure River watershed were investigated, for the first time, using sediment cores collected from two ponds near the outlet. As recently raised by Bábek et al. (2020), the spatial distribution of sediments in the depositional zones (behind a dam in the case of this study) and thus the spatial distribution of sediment-associated contaminants, is rarely studied. In addition, it is generally accepted that the studied sediment core is representative of the watershed signals, but without the absolute certainty that a local disruption could have disturbed the global recorded signal. Hence, it is difficult to know if the studied sediment core is representative of (i) the whole depositional zones and, (ii) the global signature of the inputs from the whole watershed. To circumvent this uncertainty, sediment cores were collected in our study in two ponds in order to ensure that

105 the recorded sedimentological and geochemical signatures are not disturbed by local inputs
106 and can be considered as representative of the whole watershed. In addition, and for each
107 ponds, the representativeness of the sediment cores was investigated with ground-penetrating
108 radar profiles. Our study also proposes an original coupling between sedimentological and
109 geochemical analyses to assess the deposition conditions and the nature of the sediment
110 deposits as they can influence the temporal trends of trace metal elements TME (Dhivert et
111 al., 2015). Lastly, the morphological changes modifying the depositional conditions have been
112 studied by using historical documentaries as seen in previous studies (Pittam et al., 2009;
113 Grygar et al., 2016).

114 Hence, combining a comprehensive set of geophysical, sedimentological, geochemical
115 methods and, historical documentaries, our main objectives were to (i) determine the
116 consequences of the morphological modifications of depositional zones during the diversion
117 of the Eure River outlet on the sedimentary dynamic, (ii) determine the nature of these legacy
118 sediment deposits and (iii) reconstruct the temporal trends of anthropogenic activities with a
119 focus on TME considered as markers of industrial activities in the Eure River watershed. This
120 study also discussed the reactivity of the watershed to anthropogenic activities, and the
121 resilience of the system to overcome these stresses.

122

123 **2. Material and Methods**

124

125 2.1. Setting

126

127 The Seine River flows into the Paris Basin. Sedimentary formations (Jurassic limestone and
128 marls, Cretaceous chalk, carbonaceous alluvial, and Tertiary quartz deposits) cover most of
129 the basin, with carbonate formations dominating (Thibert, 1994). The Eure River watershed

(Figure 1B) is underlain by a chalk formation from the Upper Cretaceous, covered by sandy-clay deposits from the Tertiary and Quaternary deposits (Quesnel, 1997; Laignel et al., 1998). The Eure River is the fourth largest tributary of the Seine Basin in terms of area (6 017 km²), and the fifth in terms of flow at the outlet (Q_{mean} = 22.1 ± 6.7 m^3 s^{-1}) for the period from 1971 to 2019 (www.hydro.eaufrance.fr).

Until the end of the nineteenth century, there were numerous islands spread through the channel of the Seine Estuary. At that time, the Eure River outlet was more than 11 km upstream of the present outlet (Figure 2A). Therefore, the studied coring sites at Martot and Les Damps did not exist (see section 2.2) and were in the left branch of the Seine Estuary, which was a dynamic riverine environment, unfavourable to sediment deposition.

Between 1861 and 1864, the Martot Dam (needle dam), the first of its scale in the Seine Estuary, was built in two parts (169.6 m + 135.0 m) across two branches of the Seine River (Figure 2B). During the 1880s, the Poses Dam was constructed further upstream (Figure 1A). These two dams were built in a section of the Seine Estuary where navigation was made difficult by the presence of the islands and natural weirs. The first major modification that impacted the Eure River dates back to the 1930s (1929–1935), when the Eure River outlet was moved 2 km downstream by following a former part of the left branch of the Seine River (Figure 2C). This morphological modification formed a pond connected to the Eure River (Les Damps Pond). The entire section was completely disrupted during the 1930s, and the channel of the Seine River was deeply restructured. During this period, the channel morphology of the Seine River was modified, in some cases by passing through former islands or by filling connections between the many islands present in its channel. Between 1937 and 1939, the Eure River outlet was moved 9 km downstream by following the former branch of the Seine River and was relocated at the Martot Dam. At the same time, a dike was built in the middle of the Martot Dam in the direction of the flow to isolate a pond (Martot Pond). In 1939, the connection between Martot Pond and the Seine River was filled to

156 calibrate the Seine River channel while a connection between Martot Pond and the Eure River
157 was opened thereafter. The Martot Dam became obsolete when the connections between the
158 islands were filled and was partially removed between 1938 and 1941, leaving only the part
159 across the branch of the Eure River (Figure 2D).
160 The area did not experience further evolution until 2017 when the Martot Dam was removed
161 following the Water Framework Directive (2000/60/CE), to facilitate the continuity of
162 sediment transport.
163
164 2.2. Sampling sites
165
166 *2.2.1. Upstream site: Les Damps Pond*
167 Les Damps Pond (formed between 1929–1935) is upstream of the Eure River spillway
168 (Figure 3A). The pond, which has an average depth of 50 cm and an area of less than 1 ha, is
169 connected to the Eure River, even during low water periods, and continually accumulates
170 suspended particulate matter (SPM) from the Eure River watershed (Figure 3B). Because the
171 site is 2 km upstream of a spillway, the tides have no noticeable effect, even in the case of a
172 high tidal coefficient.
173 The cores were extracted from this pond in January 2015 and 2017, using a gravity corer
174 (UWITEC) and PVC tubes with a diameter of 90 mm. The water-sediment interface was
175 preserved during coring (Table 1).
176
177 *2.2.2. Downstream site: Martot Pond*
178 Cores were also extracted from Martot Pond (area ~ 7 ha), in the lower reaches of the study
179 area (Figure 3A). Martot Pond is affected by the waters of the Seine River during tidal flows
180 through the Eure River outlet. However, the impact of the tide is limited and temporally
181 variable, as its flow persists for about 3 h and does not occur every day, because the dam,

located 200 m downstream from the connection with this pond, stops tidal flows for tidal coefficients lower than 70 (until the removal of the dam in 2017) (Figure 3C). Thus, to ensure Martot Pond was not impacted by the Seine River flow, results from this core site were compared with those from Les Damps Pond. The Martot Dam also regulated the water level in the river and the latter was continuously connected to the Martot Pond, even during periods of low flow.

The cores were extracted from this pond in January and May 2015 and February 2017, using a gravity corer (UWITEC) and PVC tubes with a diameter of 90 mm. The water-sediment interface was preserved during coring (Table 1).

2.3. Geophysical investigation: GPR

Ground penetrating radar (GPR) is a non-invasive geophysical technique that detects electrical discontinuities. It is based on the generation, transmission, propagation, reflection, and reception of discrete pulses of high frequency electromagnetic energy (MHz). For several years, it has been particularly used in the study of sedimentary structures and deposition environments in fluvial environments (Huggenberger et al., 1994; Asprion and Aigner, 1999; Beres et al., 1999; Bristow and Jol, 2003; Neal, 2004; Kostic et al., 2005; Huggenberger and Regli, 2006; Bábek et al., 2008; Słowik, 2015; Gu et al., 2019). In this study, the surveys were carried out in an aquatic environment (Water GPR-WGPR) because it is possible to tow the antennas of the geological radar in or behind a boat (Mellett, 1995; Lin et al., 2009; Sebok et al., 2018). The GSSI SIR 4000 acquisition system (Geophysical Survey System Inc., Salem, USA) was connected to a Trimble GPS with a 400 MHz antenna. The instrumentation was loaded on a high density polyethylene boat. A total of five longitudinal profiles was acquired closest to the sampled cores, at both of the two sites (Figures 3B & 3C). The data were processed with Radan 7 software (GSSI copyright) to obtain interpretable radargrams. A

208 velocity of 0.075 m ns^{-1} was determined using the hyperbola method and the correlation with
209 sediment cores. This is of the same order of magnitude as the measurements made by Lin et
210 al. (2009) (0.076 m ns^{-1}) and O'Driscoll et al. (2010) (0.06 m ns^{-1}) on comparable sediments.
211
212 2.4. Sedimentological analysis
213
214 *2.4.1. Grain size distribution*
215 The grain size distribution can influence the behaviour of chemical compounds. Radioactive
216 tracers (^{210}Pb, ^{137}Cs, and ^{241}Am) are preferentially adsorbed onto fine particles (Livens and
217 Baxter, 1988; Walling and Woodward, 1992; Wang and Cornett, 1993; He and Walling, 1996;
218 Monna et al., 1998; Gil-García et al., 2009) as well as organic and metallic contaminants
219 (Horowitz and Elrick, 1987; Walling et al., 2003; Grosbois et al., 2006; Devault et al., 2009;
220 Coynel et al., 2016). Thus, the grain size distribution can have a considerable impact on
221 radioactive tracers and TME concentrations along sediment cores (He and Walling, 1996).
222 Differences in grain size are also excellent indicators of flood events or anthropogenic
223 activities (e.g. changes in land use) (Kurashige and Fusejima, 1997; Weltje, 2012; Toonen et
224 al., 2015; Collins et al., 2017).
225 The grain size distribution of the sediment cores was measured by laser diffraction (LS
226 13320 Particle Size Analyser Beckman Coulter™). The measurements were realised every cm
227 by integrating 1 cm on the DAM15-02 and MAR15-01 cores.
228
229 *2.4.2. Total organic carbon content*
230 The total organic carbon (TOC) and organic matter (OM) quality can also influence TME
231 concentrations (Audry et al., 2006; Tseng et al., 2001; Masson et al., 2011; Petit et al., 2013;
232 Coynel et al., 2016). Moreover, variations in TOC and related parameters (e.g. HI and OI)
233 provide information on the hydrological dynamics and anthropogenic impact in a watershed.

234 The TOC content was measured using Rock-Eval 6 (RE6) pyrolysis ("Turbo" model RE6
235 pyrolyzer, at the ISTO laboratory, University of Orléans), as described in Copard et al.
236 (2006). The OM quality was obtained from measuring HI (hydrogen index, in mg HC g^{-1}
237 TOC) and OI (oxygen index, in mg O_2 g^{-1} TOC). HI corresponds to the quantity of HC
238 released relative to TOC, while OI reflects the quantity of oxygen released as CO and CO2
239 relative to TOC. Used together, these two parameters in the pseudo Van-Krevelen diagram
240 (HI vs OI) can support the identification of the OM origin and its subsequent processes
241 (Tissot and Welte, 1984). These variables were measured on the DAM17-02 (at intervals of 2
242 cm) and MAR15-01 cores (at intervals of 1 cm).
243
244 *2.4.3. Magnetic susceptibility*
245 The magnetic properties of accumulated stored sediments are generally used to identify
246 detrital inputs (e.g. from floods) (Debret et al., 2010) and anthropogenic modifications (e.g.
247 metallic pollution in soils and sediments) (Hanesch and Scholger, 2002; Knab et al., 2006;
248 Magiera et al., 2006; Blaha et al., 2008). The magnetic properties of the sediment can also be
249 used to determine the origin of the particles (Caitcheon, 1998; Hatfield and Maher, 2008,
250 2009; Hatfield and Stoner, 2013; Collins et al., 2017).
251 The magnetic susceptibility (MS) of the cored sediments was measured using a Bartington
252 MS2E point sensor as described in Debret et al. (2010). The MS of the sediment from the
253 DAM15-02, DAM15-03, DAM17-02, MAR15-01, and MAR15-05 cores was determined.
254
255 *2.4.4. Spectrocolorimetry*
256 Various parameters that can be determined using a spectrocolorimeter, such as reflectance
257 (L*) and the first derivative reflectance spectra (FDS), may be used to determine the nature
258 and the origin of sediment deposits, and sediment dynamics (Debret et al., 2006, 2011; Sebag
259 et al., 2013). L* describes the lightness of the sediment without any information on the nature

of the sediment. FDS provides qualitative information about the major components (such as clay and carbonates) of the sediment deposits. The Q7/4 diagram (700 nm/400 nm ratio vs L*) proposed by Debret et al. (2011) is used to determine the sedimentary dynamics.

A Konica Minolta CM 2600d was used to measure the intensity of the reflectance of the sediment in the visible domain (360–740 nm with a spacing of 10 nm) as described in Debret et al. (2011).

These measurements were obtained for the DAM15-02, DAM15-03, DAM17-02, MAR15-01, MAR15-02, MAR15-03, MAR15-04, MAR15-05, and MAR16-02 cores.

2.5. Geochemical analysis by XRF core scanning (XRF-CS)

X-Ray fluorescence spectrometry (XRF) is used to determine the major and trace element composition of sediment deposits (Richter et al., 2006). The XRF core scanning data can be used to describe particular TME contamination in sediment cores (Battiston et al., 1989; Dickinson et al., 1996; Lepland et al., 2010; Sabatier et al., 2014; Guédron et al., 2016; Hennekam et al., 2019). The data presented were normalised by Ti (considered as a better "normalising element" than Al) to remove possible variations because of detrital inputs (Kylander et al., 2011; Duan et al., 2014; Bábek et al., 2015; Chawchai et al., 2016).

The relative contents of the major and trace elements were measured using an XRF Avaatech core scanner (EDYTEM, University of Savoie Mont Blanc). An X-Ray beam was generated with a rhodium anode and a 125 μm beryllium window, which allows a voltage range from 7 to 50 kV and a current range of 0 to 2 mA. The analytical settings were adjusted at 10 kV and 1 mA to detect light elements, and trace elements (namely Pb, Cu, Zn, and Ni) were detected in a second run, performed at 30 kV for 0.75 mA. Each individual power spectrum was transformed by deconvolution into its relative contents (intensities), expressed

285 in counts per second (cps). Measurements were realised every 5 mm for the MAR15-01 and
286 DAM17-02 cores and every 2 mm for the MAR16-02 and DAM15-02 cores.
287
288 2.6. TME analysis
289
290 Microwave-assisted sediment digestion for particulate trace metal analysis (Pb, Zn, Cu,
291 presented in this study) was performed on samples collected in the MAR16-02 core (0.5 g of
292 dry, powdered and homogenised sediment) with aqua regia (HNO_3: 3 mL TraceMetal™
293 Grade; HCl: 9 mL TraceMetal™ Grade). Following the mineralisation, the solutions were
294 diluted in 100 ml of Milli-Q® water. Particulate trace metal concentrations were measured by
295 inductively-coupled-plasma atomic emission spectroscopy (ICP-AES) (iCAP 6000 Series,
296 Thermo Fischer®) performed with external calibration. The accuracy and precision of the
297 measurements were checked against a certified reference material (Trace Element on Fresh
298 Water Sediment CNS301-04-050, Sigma Aldrich) and the results showed accuracies of ≥ 98
299 % with a precision of ≤ 4 % (RSD). All of the analyses were carried out in triplicate (standard
300 deviation ≤ 1.1 %).
301
302 2.7. Short-lived radionuclides
303
304 The activities of ^{210}Pb in excess ($^{210}Pb_{ex}$), ^{137}Cs, and ^{241}Am were determined on samples
305 from the MAR15-01 core (at steps of 1, 4, or 6 cm) using a germanium spectrometer with
306 ultra-low background noise at the Laboratoire Souterrain de Modane (LSM). The age model
307 was computed with the *serac* R package (https://github.com/rosalieb/serac, (Bruel and
308 Sabatier, Submitted).
309
310 **3. Results**

311

312 3.1. Sedimentological characterisation of the sediment cores

313

314 *3.1.1. Les Damps Pond*

315 The sediment cores all showed similar sedimentary facies called U1 (Figures 4A1 & 4A2).
316 The grain size distribution was homogeneous (median (D_{50}) = 29.5 ± 6.7 µm) and showed
317 only one population, centred around the D_{50}. (Figure 4B). The TOC content was high and
318 constant (TOC_{mean} = 5.36 ± 0.47 %). HI and OI were also constant, and the values of HI were
319 higher than those of OI (HI_{mean} = 302 ± 23 mg HC g^{-1} TOC and OI_{mean} = 145 ± 10 mg O_2 g^{-1}
320 TOC) (Figure 4C).

321 The MS values were high and constant between 60 and 90 cm (MS_{mean} = 12 ± 2) but had a
322 peak at 50–60 cm. The values decreased between 50 and 30 cm and were constant above 30
323 cm (MS_{mean} = 6 ± 1) (Figure 4D).

324 The values of L* were low and constant (L^*_{mean} = 28.5 ± 2.3 %), with values between 22
325 and 38 % (Figure 4D).

326 The intensities of FDS were high at wavelengths between 675 and 735 nm. This signature
327 was continuous, and the intensity did not vary, which may mean that the origin of the
328 sedimentary inputs remained the same throughout the sedimentation (Figure 4E).

329 The Pb/Ti ratio was low and constant (Pb/Ti_{mean} = 0.64 ± 0.12) between 30 and 80 cm but
330 increased at 30 cm. The values of the ratio were generally high between 0 and 30 cm
331 (Pb/Ti_{mean} = 2.26 ± 0.58) and decreased from 15 cm to the surface (Figure 4F). The Zn/Ti,
332 Cu/Ti, and Ni/Ti ratios showed the same trend. These three ratios were high between 30 and
333 80 cm and reached maximum values between 50 and 60 cm (Zn/Ti_{mean} = 2.04 ± 0.24,
334 Cu/Ti_{mean} = 1.43 ± 0.71, and Ni/Ti_{mean} = 0.04 ± 0.01). Around 30 cm, the ratios decreased and
335 were constant between 0 and 30 cm (Figure 4F).

336

337 *3.1.2. Martot Pond*

338 The sediment cores showed two sedimentary facies delimited by a transition zone at 75–80
339 cm. In this section, the results from the MAR15-01 core are presented. The upper facies (0–75
340 cm) is referred to as U1, while the lower facies (75–138 cm) is referred to as U2 (Figure 5A).

341 • U2 facies:

342 The grain size distribution was homogeneous (median (D_{50}) = 13.8 ± 7.0 µm) and showed
343 one population centred around D_{50} (Figure 5B). The TOC content was low and constant
344 (TOC_{mean} = 1.75 ± 0.33 %). HI was constant (HI_{mean} = 147 ± 24 mg HC g^{-1} TOC) and lower
345 than OI (OI_{mean} = 260 ± 35 mg O_2 g^{-1} TOC). OI increased, peaked at 103.5 cm (OI = 347 mg
346 O_2 g^{-1} TOC), then decreased. The only exception to this trend was at the depth of 128.5 cm
347 (Figure 5C).

348 The MS was low and L* was high and constant (L^*_{mean} = 44.4 ± 2.1 %), with values
349 between 40 and 50 % (Figure 5D).

350 The intensities of FDS were high for wavelengths between 365 and 550 nm. A second
351 signature, less intense, was also visible for high wavelengths (675–735 nm). This indicates
352 that several signatures were marked within the facies and the small variations in intensity
353 suggest the origin of the whole U2 facies was unique (Figure 4E).

354 The Pb/Ti, Zn/Ti, Cu/Ti, and Ni/Ti ratios were low and constant (Pb/Ti_{mean} = 0.33 ± 0.10,
355 Zn/Ti_{mean} = 0.54 ± 0.11, Cu/Ti_{mean} = 0.18 ± 0.05, and Ni/Ti_{mean} = 0.04 ± 0.01) and were higher
356 only at the transition between the two facies in the 75–80 cm depth interval (Figure 5F).

357 • U1 facies:

358 The grain size distribution was homogeneous (median (D_{50}) = 33.9 ± 7.8 µm) and had one
359 population centred around D_{50} (Figure 5B) as in Les Damps Pond. The TOC content was
360 twice as high in U1 (TOC_{mean} = 3.88 ± 1.49 %) as in U2, and the values were particularly high

361 near the top of the core (TOC = 8.26 ± 0.19 % between 9 and 12 cm). HI increased upwards
362 from the transition between U1 and U2 and stabilised at a depth of 66.5 cm. OI continued to
363 decrease in U1 and stabilised at a depth of 66.5 cm in U1. At the opposite end of the U2
364 facies, HI was high (HI_{mean} = 279 ± 23 mg HC g^{-1} TOC) and OI was low (OI_{mean} = 150 ± 17
365 mg O_2 g^{-1} TOC) (Figure 5C) as described along the U1 facies in Les Damps Pond.
366 The U1/U2 transition was marked by a strong increase in MS and a decrease in L*. The MS
367 values were high (MS_{mean} = 25 ± 7) from 45 to 75 cm but were lower (MS_{mean} = 8 ± 4)
368 between 0 and 45 cm (Figure 5D). The L* was lower in the U1 facies ($L^*_{mean.}$ = 34.1 ± 4.2 %)
369 than in the U2 facies, and was almost the same as the values between 24 and 40, and
370 decreased next to the top of the core (Figure 5D). The sediment colour was similar to that in
371 the U1 facies in Les Damps Pond.
372 The intensities of FDS were high at high wavelengths (675–735 nm), but, unlike the U2
373 facies, low wavelength signatures were not noticeable. This indicates a major change in the
374 nature of the sediment stored in Martot Pond (Figure 5E). Moreover, the signature was
375 continuous and the intensity did not vary as in Les Damps Pond.
376 The Pb/Ti ratio increased at the U1/U2 transition but remained stable to a depth of 35 cm
377 (Pb/Ti_{mean} = 1.06 ± 0.15 between 35 and 75 cm). The ratio was higher from 35 to 10 cm
378 (Pb/Ti_{mean} = 3.17 ± 0.53 between 10 and 35 cm) and trended to decrease closer to the top of
379 the core (Figure 5F). The patterns in the Zn/Ti, Cu/Ti, and Ni/Ti ratios were similar. Indeed,
380 from the transition between U1 and U2, the ratios increased and peaked between 50 and 60
381 cm (Zn/Ti_{mean} = 4.79 ± 0.73, Cu/Ti_{mean} = 1.19 ± 0.20, and Ni/Ti_{mean} = 0.11 ± 0.01). The ratios
382 decreased from 50 to 35 cm and then stabilised above 35 cm (Figure 5F). The variations in the
383 Pb/Ti, Zn/Ti, Cu/Ti, and Ni/Ti ratios generally followed a similar pattern to those described
384 for Les Damps Pond.
385
386 3.2. TME concentrations along the U1 facies in Martot Pond

387

388 The trends in the Pb/Ti, Zn/Ti, and Cu/Ti ratios for the top 77 cm of the MAR16-02 core
389 and the U1 facies of the MAR15-01 core were similar, which shows that this facies was also
390 well represented within MAR16-02. The Pb, Zn, and Cu concentrations were measured at the
391 depths for which the XRF ratios reached maximum and minimum values within the MAR16-
392 02 core (Figure 6).

393 The Pb concentration was constant to a depth of 35 cm (Pb_{mean} = 120 ± 28 mg kg^{-1}), apart
394 from at 65 cm (Pb = 190 mg kg^{-1}). The Pb concentrations increased in the same way as the
395 Pb/Ti ratio, and the concentrations were highest at 12 cm (Pb = 669 mg kg^{-1}). Near the top of
396 the core (4 cm), the Pb concentration decreased, similar to the Pb/Ti ratio, and at 299 mg kg^{-1}
397 it was less than half the maximum concentration at 12 cm but almost 2.5 times the average
398 concentration below 35 cm (Figure 6). The Zn and Cu concentrations were 415 mg kg^{-1} and
399 113 mg kg^{-1} at 77 cm, respectively. The concentrations of these two TMEs peaked at 65 cm
400 (Zn = 905 mg kg^{-1}, Cu = 399 mg kg^{-1}). Between 10 and 40 cm, the Zn and Cu concentrations
401 were less than half and less than a quarter of the maximum concentrations, respectively, and
402 the Zn/Ti and Cu/Ti ratios were also low close to the top of the MAR16-02 core (Figure 6).
403 The Zn and Cu concentrations at 4 cm were lower than those measured at 77 cm.

404

405 3.3. Age model of the MAR15-01 core

406

407 Recent deposit dating and sedimentation rate estimates have been realised from short-life
408 radionuclides (Robbins and Edgington, 1975; Appleby and Oldfield, 1978; Appleby et al.,
409 1991; He and Walling, 1996; Mabit et al., 2014). The sedimentation rate was determined from
410 the $^{210}Pb_{ex}$ by subtracting the ^{226}Ra activity from the $^{210}Pb_{total}$ (Krishnaswamy et al., 1971).
411 The ^{137}Cs and ^{241}Am activities were used to identify nuclear weapon testing with maximum

activity in 1963, and the Chernobyl accident in 1986 and are used to confirm the age model established with $^{10}Pb_{ex}$.

The activity of $^{210}Pb_{ex}$ was measured to 80 cm and decreased almost continuously with depth. A sedimentation rate of 12.73 mm y^{-1} (R^2 = 0.60) was estimated using the 'constant flux, constant sedimentation rate' (CFCS) model (Krishnaswamy et al., 1971) (Figure 7A). The ^{137}Cs and ^{241}Am activities peaked at 60 and 58 cm, respectively, corresponding to the maximum fallout from atmospheric nuclear weapon testing in 1963 (Robbins and Edgington, 1975; Appleby et al., 1991) (Figure 7B). There was also a peak in the ^{137}Cs activity at 40 cm, perhaps related to the Chernobyl accident in 1986 (Figure 7B). An age model was realised for the U1 facies of the MAR15-01 core using the sedimentation rate obtained from the $^{10}Pb_{ex}$ (Figure 7C).

4. Discussion

4.1. Sedimentary filling in the depositional zones

As the sedimentological parameters are presented for one core from Martot Pond (two cores in the case of Les Damps Pond), it is essential to ensure that the studied cores are representative of sediment records in the entire respective pond. Concerning Martot Pond, a sediment thickness between 2.0–2.5 m is showed by the radargram GPR_MAR_08 (Figure 8A). The reflector R1 made it possible to distinguish two islands without a well-differentiated structure on this scale, which may correspond to parts of the central island that separated the two branches of the Seine River (Figure 2). A second reflector (R2, solid red line) between 350 m and 550 m separates U1 and U2 and this interpretation is justified by the MAR15-02 core in which this limit is observed at 85 cm (corresponding to the transition between U1 and U2 observed on MAR15-01 core at 75–80 cm). Beyond this section, it is more difficult to

438 locate R2, but the position of the MAR15-03, MAR15-04 and MAR15-06 cores, with the aid
439 of some clues, allowed us to position R2 (red dotted line). Geophysical prospecting shows a
440 homogeneous filling within Martot Pond and thus validates the representativeness of the
441 studied core.

442 Concerning Les Damps Pond, two quality profiles have been obtained (Figures 8B & 8C) in
443 which a reflector (R3) showed the lower limit of U1. In this facies, few continuous structures
444 were detectable, probably because of the fine accumulated sediments and the monotony of the
445 sediment as observed in the DAM15-02 and DAM17-02 cores. However, under R3, it was
446 possible to distinguish less powerful reflectors, probably attributed to the presence of a bed of
447 coarser material (Figure 8B). This reflector was therefore interpreted as the upper limit of the
448 former stream-bed of the Seine River. Hence, the two studied sediment cores are
449 representative of the sedimentary records of the entire pond.

450

451 4.2. Identification of the deposition conditions and sediment origin

452

453 The grain size in the U2 facies (D_{50} = 13.8 ± 7.0 µm) of Martot Pond and in the U1 facies of
454 Martot and Les Damps Ponds (D_{50} ~ 30 µm) suggests a weak sedimentation dynamic, that is,
455 deposition under very low flow conditions, but also suggests two distinct unidentified origins.
456 U2 was also characterised by an HI/OI ratio <1 (Figure 9A), reflecting the input of material
457 from a terrestrial origin (Carrie et al., 2012). In detail, the values of these two indicators of
458 OM quality reflect an organo-mineral soil horizons origin (A horizon) (Disnar et al., 2003).
459 Conversely, the U1 facies of both ponds are characterised by an HI/OI ratio of approximately
460 2 (Figure 9A), suggesting that the OM origin is either aquatic (Carrie et al., 2012) or, with
461 respect to the HI and OI values, detrital (OH or A horizons) (Disnar et al., 2003). Therefore,
462 OM in the U1 facies is less altered and may have a mix aquatic/terrestrial origin, than that
463 stored in the U2 facies.

Spectrocolorimetry data for U2 showed a sedimentary dynamic mainly structured around two end-members which are poles “clayey deposits” and “carbonate deposits” (Figure 9B). The clayey deposits pole reflects the input of detrital clay sediments while the carbonate deposits pole reflects the input of light sediments because of their carbonate contents. These results were confirmed by FDS and show a predominance of the carbonate signature (Debret et al., 2011). The U2 facies is therefore the consequence of the sedimentation of a clay-carbonate material, with an organic component that had a terrestrial origin. This terrigeneous deposit, which accumulated in a low intensity zone, may be derived from the erosion of the carbonate substratum of the Seine River watershed.

In terms of the U1 facies of both ponds, there was sedimentation consisting of fine sediments enriched in OM. Indeed, the U1 facies is close to the poles of “clayey deposits” and “organic-rich sediment (*Chlorophyll-a and by-products*)” (Figure 9B). This organic pole, also confirmed by the FDS (Debret et al., 2011), could be explained by high aquatic primary production and also by a less degraded soil OM. Such mixing is also verified by the pseudo Van-Krevelen diagram.

The similar trend of the U1 facies from the two ponds, and the absence of a clear depth distribution in the pseudo Van-Krevelen and Q7/4 diagrams (Figure 9), suggest that (i) SPM are not altered by any processes between the ~10 km separating the two ponds and, (ii) sediment deposits were not submitted to post-depositional alterations (e.g., early diagenesis), probably due to a high sedimentation rate (Van Metre et al., 1997; Horowitz et al., 1988; Callender and Robbins, 1993; Callender, 2000; Audry et al., 2004). Hence, there is a common origin of sediments from both U1 facies, corresponding to the inputs from the Eure River (U1 = Eure Unit) and consequently, intrusions of the Seine River into Martot Pond (during tidal flow) do not alter the Eure River signature. Therefore, the U1 facies from Martot Pond was considered as representative of the Eure River signal recorded in sediments, and so was used to build an age model.

490

491 4.3. Links with the morphological modification of the Seine and Eure Rivers

492

493 According to the age model established for the MAR15-01 core, the transition between the
494 U2 facies and the Eure Unit date from around 1954 ± 10 y. The history of the study site
495 showed that Martot Pond was disconnected from the Seine River from 1939. The recently
496 shaped connection between Martot Pond and the Eure River seems consistent with this
497 change, or else dated from the early 1940s. The age model therefore seems consistent with the
498 morphological modification, and the facies change was established at 1939–1944, when
499 Martot Pond was isolated from the Seine River.

500 The U2 facies was deposited before this major change. The history of the study site shows
501 that, before the Eure River oulet was diverted, the present Martot Pond corresponded to the
502 area behind the Martot Dam, supplied by waters from the Seine River. The U2 facies
503 corresponds to sedimentation of material from the Seine River watershed upstream of the
504 dam. Moreover, the GPR prospecting showed that, in some places, the potential lower limit of
505 this unit corresponded to parts of the island seperating the two branches of the Seine River.

506 The sediment stored in Martot Pond would be useful to study the Eure River basin from the
507 early 1940s. However, the lack of dating means that, to date, the U2 facies (Seine Unit) has
508 not been analysed in detail and will be the subject of a future prospsection.

509

510 4.4. Identification of an anthropogenic imprint in the Eure River facies

511

512 According to the correlation matrix, the major elements (Si, Fe, Al, and Ti) were strongly
513 correlated with each other ($0.69 < R < 0.87$) (Figure S1). The input of these major elements
514 represents the detrital inputs from the Eure River watershed. The trace elements (Zn, Cu, Ni,
515 and Pb) were not correlated with major elements, demonstrating that their presence within the

516 Eure Unit was not linked to the natural input of the Eure River watershed. In addition, Zn, Cu,
517 and Ni were positively correlated with each other ($0.79 < R < 0.88$), indicating a common
518 source in the watershed (Figure S1). The lack of correlation between TME and fine particles,
519 as well as the homogeneity of the grain size distribution, indicates that the TME variations
520 were related to anthropogenic contributions rather than lithological variations. This lack is
521 also seen with the OM, because the variation in TOC vs TME is not correlated. Lastly, the
522 sedimentation rate does not control the TME variations, as the latter was estimated as constant
523 over the considered period.
524 As a consequence, the temporal variations in the semi-quantitative Zn, Cu, Ni, and Pb data
525 were related to changes in the input of particulate TME. These variations may reflect the
526 presence of new sources within the watershed, and may be related to anthropogenic activities
527 that occurred during the second half of the twentieth century.
528
529 4.5. Reconstruction of Pb history
530
531 In large European watersheds, Pb levels generally exhibit similar temporal trends with
532 increases from the 1940s until the 1970s, then decreases until the 1990s (Danube and Rhine
533 Rivers : Winkels et al., 1998; Loire River : Grosbois et al., 2006; Seine River : Le Cloarec et
534 al., 2011; Ayrault et al., 2012; Rhône River : Ferrand et al., 2012). Conversely, in the Eure
535 River, Pb levels were stable during the 1960s, increased at the end of the 1980s, and reached a
536 maximum in the 1990s and 2000s followed by a decrease after 2006 (Figure 10). The high
537 Pb/Ti ratio values in Martot Pond in the 1990s and 2000s reflect the high Pb concentrations
538 measured along the MAR16-02 core. This high concentration was also seen in SPM and
539 dissolved load collected in the lower reaches of Eure River from March and September 2009
540 (Chiffoleau et al., 2012). In detail, the concentrations were 4–5 times (for particulate
541 concentrations: Pb_p = 430 and 380 mg kg^{-1}; measured on SPM) and 5–10 times (for dissolved

concentrations: Pb_d = 1400 ng L^{-1} and 800 ng L^{-1}) higher than those measured in the Seine River at Poses and during the same period. Chiffoleau et al. (2012) hypothesised that the high Pb levels were not related to atmospheric input but rather to a cathode-ray tube (CRT) factory containing 1 to 3 kg of Pb (Tsydenova and Bengtsson, 2011) in their leaded glass (Singh et al., 2016). The CRT factory started operating at Dreux in 1956 and a second factory, specialising in the assembly of CRT TVs and the manufacture of electrical circuits, opened in 1974 in the same industrial site. The Pb content in the sediments showed little evidence of the successive commencement of these two factories (Figure 10). The industrial production increased from 1990 to the 2000s, when the factories were taken over by the Philips Group, increasing the Pb discharge from the site. To illustrate our statement, the European Environment Agency reported a direct release of 3540 kg of Pb into the water in 2001, exposing it as one of the highest European Pb emitters. Between 2002 and 2005, production decreased, as did Pb release (1900 to 1500 kg of Pb into the water in the years 2003 and 2004) ("IREP," n.d.). At the commencement of industrial growth, the Pb/Ti ratio began to increase, and reflecting the instantaneous reactivity of the watershed to this anthropogenic disturbance. However, the fall in industrial output did not produce a decrease in the Pb/Ti ratio, which continued to rise into the late 2000s when the industrial sites were definitively closed (Figure 10). Again, this signifies that the watershed reacts to anthropogenic changes, however, the decrease in the ratio is slower than initially expected and remains high after the termination of industrial activity. As an example, near the top of the core, the Pb concentration is twice as high as than the average concentration estimated before 1990. As the levels of the Pb/Ti ratio and the Pb concentrations before industrial activity increased (1990s) may correspond to a reference level of Pb concentration in the Eure River, an additional Pb source is expected in the Eure River watershed. Without any other anthropogenic Pb emitters, it is reasonable to conjecture that this is likely related to Pb contaminated soil surrounding the factory and Pb contaminated sediments stored in the riverbanks and channel, which fed Pb into the river

during erosion processes. Hence, the watershed was not able to react immediately to the cease of industrial activity, and a resilience period of the system could be identified (Holling, 1973; Folke et al., 2002). In this case, and due to the erosion of contaminated soil and sediments further realising Pb into the environment, it will be take several years or decades for the river to reach the reference level in Pb concentration. The close relationship between this industrial activity and the observed temporal trends in Pb content suggests that this activity is the main source of contamination but does not allow to state that it is the only one.

4.6. Reconstruction of Zn, Cu, and Ni

First, the sharp increase in Zn, Cu, and Ni at the transition between the Seine and the Eure Units shows how the modification of the Seine River channel (for navigation) instantly impacted the quality of the sediments deposited in Martot Pond. The historical trends of Zn, Cu, and Ni, reported by several studies in large European rivers, such as the Danube, Rhine, Loire and Seine basins, show that the concentrations increased between 1940 and the 1970s, then decreased (Winkels et al., 1998; Grosbois et al., 2006; Le Cloarec et al., 2011). Just as in these watersheds, the Zn, Cu, and Ni contents in the Eure River watershed were high until the 1980s and peaked during the 1960s and 1970s (Figure 10). The strong correlations between these elements suggest a single source to the Eure River, that started before the facies transition, with the Wonder battery factory the likely source. This factory near the Eure River (20 km upstream from Les Damps) manufactured saline batteries (from Zn) and supplied nearly 40 % of the national market in 1966. The history of this industrial activity indicates that in 1971, the factory was the subject of an increased administrative survey by a national agency, prompting reduced discharge into the Eure River (Agence Financière de Bassin "Seine-Normandie," 1971). This survey is recorded in the sedimentary archive and corresponds to the beginning of the decrease in Cu (Figure 10). Due to a global evolution of

the industry (relocation, change in type of batteries), this industry declined in the late 1960s, which is reflected in the Zn, Cu, and Ni contents in the sediments. After the termination of industrial activity (1994), the Zn, Cu, and Ni content remains stable. Here, the watershed seemed to react instantly with the change in anthropogenic activity. Even if we had no historical and industrial arguments to state that this industrial site was the single source of TME in the river, we would suggest that it was the main one, which is supported by the close relationship between its activity and the observed trends in Zn, Cu, and Ni content in the studied core.

The stability of the ratios may indicate that TME release has ceased, but this has to be monitored as there is no record of the TME concentrations before the factory opened in 1938 (Guermond, 1981). Hence, it is therefore impossible to confirm whether the pre-contamination levels have been restored or whether contaminants are still being released, even at lower levels, as was the case for Pb.

5. Conclusion

The modification of the Seine River morphology since the nineteenth century has generated depositional zones in the lower Eure River. The transition between the Seine River and the Eure River units was the marker of one of the last main morphological changes undertaken in the Seine River Estuary.

A geophysical investigation of both ponds showed a homogeneous filling validating the representativeness of the studied sediment cores. Consequently, our results revealed a regional signature and are not linked to some local conditions.

The sedimentary dynamic during deposition and the nature of the sediment were determined to ensure that the TME evolution over time was related to anthropogenic activities.

The study of legacy sediments allowed the reconstruction of the industrial trajectory of the watershed since the 1940s. Our results suggested that the Eure River watershed was submitted to high human pressures that could have affected the Seine Estuary.

We have demonstrated that the watershed is very sensitive to any disturbance though a resilience period occurs that extends beyond the period of these disturbances, due to erosion of contaminated soil and sediment.

In the course of the Anthropocene, sedimentation zones containing contaminated sediments may be impacted by extreme events (e.g. floods) or modified by human activities (e.g. dam destruction, dredging, and channelisation), which may cause a resuspension of these sediments within rivers, constituting a new source of contamination. Such complex processes concern most worldwide rivers, and for the foreseeable future, it will become necessary to determine their own resilience periods.

Acknowledgements

This project (OSS 276) was financially supported by the Seine-Normandie Water Agency and the Region Normandie.

Authors thank “Voie Navigable de France” and the “Batellerie” Museum for the access to their historical maps and documents.

References

Agence Financière de Bassin “Seine-Normandie,” 1971. Délibération n°71-16 du 21 Octobre 1971 désignant les entreprises industrielles soumises à la mesure pour le calcul de leur redevance pollution.

Appleby, P.G., Oldfield, F., 1978. The calculation of lead-210 dates assuming a constant rate of supply of unsupported 210Pb to the sediment. CATENA 5, 1–8. https://doi.org/10.1016/S0341-8162(78)80002-2

Appleby, P.G., Richardson, N., Nolan, P.J., 1991. 241Am dating of lake sediments. Hydrobiologia 214, 35–42. https://doi.org/10.1007/BF00050929

Ashley, J.T.F., Bushaw-Newton, K., Wilhelm, M., Boettner, A., Drames, G., Velinsky, D.J., 2006. The Effects of Small Dam Removal on the Distribution of Sedimentary Contaminants. Environ. Monit. Assess. 114, 287–312. https://doi.org/10.1007/s10661-006-4781-3

Asprion, U., Aigner, T., 1999. Towards realistic aquifer models: three-dimensional georadar surveys of Quaternary gravel deltas (Singen Basin, SW Germany). Sediment. Geol. 129, 281–297. https://doi.org/10.1016/S0037-0738(99)00068-8

Audry, S., Blanc, G., Schäfer, J., Chaillou, G., Robert, S., 2006. Early diagenesis of trace metals (Cd, Cu, Co, Ni, U, Mo, and V) in the freshwater reaches of a macrotidal estuary. Geochim. Cosmochim. Acta 70, 2264–2282. https://doi.org/10.1016/j.gca.2006.02.001

Audry, S., Schäfer, J., Blanc, G., Jouanneau, J.-M., 2004. Fifty-year sedimentary record of heavy metal pollution (Cd, Zn, Cu, Pb) in the Lot River reservoirs (France). Environ. Pollut. 132, 413–426. https://doi.org/10.1016/j.envpol.2004.05.025

Ayrault, S., Lorgeoux, C., Moilleron, R., Lherm, D., Tassin, B., Bonté, P., Roy-Barman, M., Le, M.-F., Lefèvre, I., Priadi, C., Evrard, O., Bordier, L., Mouchel, J.-M., Eurin, J., Tamtam, F., Dinh, T., Boust, D., Vrel, A., 2010b. Archives sédimentaires, empreintes des micropolluants sur le bassin de la Seine sur 80 ans. PIREN-Seine Rapp. Act. 2010 34.

Ayrault, S., Priadi, C.R., Evrard, O., Lefèvre, I., Bonté, P., 2010a. Silver and thallium historical trends in the Seine River basin. J. Environ. Monit. 12, 2177–2185. https://doi.org/10.1039/C0EM00153H

Ayrault, S., Roy-Barman, M., Le Cloarec, M.-F., Priadi, C.R., Bonté, P., Göpel, C., 2012. Lead contamination of the Seine River, France: Geochemical implications of a historical perspective. Chemosphere 87, 902–910. https://doi.org/10.1016/j.chemosphere.2012.01.043

Bábek, O., Grygar, T.M., Faměra, M., Hron, K., Nováková, T., Sedláček, J., 2015. Geochemical background in polluted river sediments: How to separate the effects of sediment provenance and grain size with statistical rigour? CATENA 135, 240–253. https://doi.org/10.1016/j.catena.2015.07.003

Bábek, O., Hilscherová, K., Nehyba, S., Zeman, J., Famera, M., Francu, J., Holoubek, I., Machát, J., Klánová, J., 2008. Contamination history of suspended river sediments accumulated in oxbow lakes over the last 25 years. J. Soils Sediments 8, 165–176. https://doi.org/10.1007/s11368-008-0002-8

Bábek, O., Kielar, O., Lenďáková, Z., Mandlíková, K., Sedláček, J., Tolaszová, J., 2020. Reservoir deltas and their role in pollutant distribution in valley-type dam reservoirs: Les Království Dam, Elbe River, Czech Republic. CATENA 184, 104251. https://doi.org/10.1016/j.catena.2019.104251

Battiston, G.A., Degetto, S., Gerbasi, R., Sbrignadello, G., 1989. Determination of sediment composition and chronology as a tool for environmental impact investigations. Mar. Chem. 26, 91–100. https://doi.org/10.1016/0304-4203(89)90054-6

Bednarek, A.T., 2001. Undamming Rivers: A Review of the Ecological Impacts of Dam Removal. Environ. Manage. 27, 803–814. https://doi.org/10.1007/s002670010189

Beres, M., Huggenberger, P., Green, A.G., Horstmeyer, H., 1999. Using two- and three-dimensional georadar methods to characterize glaciofluvial architecture. Sediment. Geol. 129, 1–24. https://doi.org/10.1016/S0037-0738(99)00053-6

Blaha, U., Appel, E., Stanjek, H., 2008. Determination of anthropogenic boundary depth in industrially polluted soil and semi-quantification of heavy metal loads using magnetic susceptibility. Environ. Pollut. 156, 278–289. https://doi.org/10.1016/j.envpol.2008.02.013

Bonté, P., Cloarec, M.-F.L., Sornein, M.-O., Lefèvre, I., Desalle, T., Mouchel, J.-M., Ayrault, S., 2004. Enregistrement sédimentaire de la contamination métallique, Piren-Seine, Rapport d'activité 2003.

Bristow, C.S., Jol, H.M., 2003. An introduction to ground penetrating radar (GPR) in sediments. Geol. Soc. Lond. Spec. Publ. 211, 1–7.

Bruel, R., Sabatier, P., Submitted. serac : a R package for ShortlivEd RAdionuclide Chronology of recent sediment cores. Quat. Geochronol.

Caitcheon, G.G., 1998. The significance of various sediment magnetic mineral fractions for tracing sediment sources in Killimicat Creek. CATENA 32, 131–142. https://doi.org/10.1016/S0341-8162(97)00057-X

Callender, E., 2000. Geochemical effects of rapid sedimentation in aquatic systems: minimal diagenesis and the preservation of historical metal signatures. J. Paleolimnol. 23, 243–260. https://doi.org/10.1023/A:1008114630756

Callender, E., Robbins, J.A., 1993. Transport and accumulation of radionuclides and stable elements in a Missouri River Reservoir. Water Resour. Res. 29, 1787–1804. https://doi.org/10.1029/93WR00387

Carrie, J., Sanei, H., Stern, G., 2012. Standardisation of Rock–Eval pyrolysis for the analysis of recent sediments and soils. Org. Geochem. 46, 38–53. https://doi.org/10.1016/j.orggeochem.2012.01.011

Chawchai, S., Kylander, M.E., Chabangborn, A., Löwemark, L., Wohlfarth, B., 2016. Testing commonly used X-ray fluorescence core scanning-based proxies for organic-rich lake sediments and peat. Boreas 45, 180–189. https://doi.org/10.1111/bor.12145

Chiffoleau, J.-F., Sonke, J.E., Auger, D., Bretaudeau, J., Joguet, T., Larrieu, M., Laffont, L., Prunier, J., Rozuel, E., Zouiten, C., 2012. Etude de la signature isotopique des métaux dans l'estuaire de la Seine. Une information essentielle pour le traçage et la discrimination des sources et processus.

Collins, A.L., Pulley, S., Foster, I.D.L., Gellis, A., Porto, P., Horowitz, A.J., 2017. Sediment source fingerprinting as an aid to catchment management: A review of the current state of knowledge and a methodological decision-tree for end-users. J. Environ. Manage., Sediment source fingerprinting for informing catchment management: methodological approaches, problems and uncertainty 194, 86–108. https://doi.org/10.1016/j.jenvman.2016.09.075

Copard, Y., Di-Giovanni, C., Martaud, T., Albéric, P., Olivier, J.-E., 2006. Using Rock-Eval 6 pyrolysis for tracking fossil organic carbon in modern environments: implications for the roles of erosion and weathering. Earth Surf. Process. Landf. 31, 135–153. https://doi.org/10.1002/esp.1319

Coynel, A., Gorse, L., Curti, C., Schafer, J., Grosbois, C., Morelli, G., Ducassou, E., Blanc, G., Maillet, G.M., Mojtahid, M., 2016. Spatial distribution of trace elements in the surface sediments of a major European estuary (Loire Estuary, France): Source identification and evaluation of anthropogenic contribution. J. Sea Res., Recent and past sedimentary, biogeochemical and benthic ecosystem evolution of the Loire Estuary (Western France) 118, 77–91. https://doi.org/10.1016/j.seares.2016.08.005

Crutzen, P.J., 2006. The "Anthropocene," in: Ehlers, E., Krafft, T. (Eds.), Earth System Science in the Anthropocene. Springer Berlin Heidelberg, Berlin, Heidelberg, pp. 13–18. https://doi.org/10.1007/3-540-26590-2_3

Crutzen, P.J., Stoermer, E.F., 2000. The Anthropocene. Int. Geosphere–Biosphere Programme IGBP 17–18.

Debret, M., Chapron, E., Desmet, M., Rolland-Revel, M., Magand, O., Trentesaux, A., Bout-Roumazeille, V., Nomade, J., Arnaud, F., 2010. North western Alps Holocene paleohydrology recorded by flooding activity in Lake Le Bourget, France. Quat. Sci. Rev. 29, 2185–2200. https://doi.org/10.1016/j.quascirev.2010.05.016

749 Debret, M., Desmet, M., Balsam, W., Copard, Y., Francus, P., Laj, C., 2006.
750 Spectrophotometer analysis of Holocene sediments from an anoxic fjord: Saanich
751 Inlet, British Columbia, Canada. Mar. Geol. 229, 15–28.
752 https://doi.org/10.1016/j.margeo.2006.01.005
753 Debret, M., Sebag, D., Desmet, M., Balsam, W., Copard, Y., Mourier, B., Susperrigui, A.-S.,
754 Arnaud, F., Bentaleb, I., Chapron, E., Lallier-Vergès, E., Winiarski, T., 2011.
755 Spectrocolorimetric interpretation of sedimentary dynamics: The new "Q7/4 diagram."
756 Earth-Sci. Rev. 109, 1–19. https://doi.org/10.1016/j.earscirev.2011.07.002
757 Devault, D.A., Gérino, M., Laplanche, C., Julien, F., Winterton, P., Merlina, G., Delmas, F.,
758 Lim, P., Miguel Sánchez-Pérez, J., Pinelli, E., 2009. Herbicide accumulation and
759 evolution in reservoir sediments. Sci. Total Environ. 407, 2659–2665.
760 https://doi.org/10.1016/j.scitotenv.2008.12.064
761 Dhivert, E., Grosbois, C., Coynel, A., Lefèvre, I., Desmet, M., 2015. Influences of major
762 flood sediment inputs on sedimentary and geochemical signals archived in a reservoir
763 core (Upper Loire Basin, France). CATENA 126, 75–85.
764 https://doi.org/10.1016/j.catena.2014.10.030
765 Dickinson, W.W., Dunbar, G.B., McLeod, H., 1996. Heavy metal history from cores in
766 Wellington Harbour, New Zealand. Environ. Geol. 27, 59–69.
767 https://doi.org/10.1007/BF00770603
768 Disnar, J.R., Guillet, B., Keravis, D., Di-Giovanni, C., Sebag, D., 2003. Soil organic matter
769 (SOM) characterization by Rock-Eval pyrolysis: scope and limitations. Org.
770 Geochem. 34, 327–343. https://doi.org/10.1016/S0146-6380(02)00239-5
771 Duan, D., Ran, Y., Cheng, H., Chen, J., Wan, G., 2014. Contamination trends of trace metals
772 and coupling with algal productivity in sediment cores in Pearl River Delta, South
773 China. Chemosphere 103, 35–43. https://doi.org/10.1016/j.chemosphere.2013.11.011
774 Evans, J.E., 2015. Contaminated Sediment and Dam Removals: Problem or Opportunity? Eos
775 96, 10. https://doi.org/doi:10.1029/2015EO036385
776 Ferrand, E., Eyrolle, F., Radakovitch, O., Provansal, M., Dufour, S., Vella, C., Raccasi, G.,
777 Gurriaran, R., 2012. Historical levels of heavy metals and artificial radionuclides
778 reconstructed from overbank sediment records in lower Rhône River (South-East
779 France). Geochim. Cosmochim. Acta, Environmental Records of Anthropogenic
780 Impacts 82, 163–182. https://doi.org/10.1016/j.gca.2011.11.023
781 Folke, C., Carpenter, S., Elmqvist, T., Gunderson, L., Holling, C.S., Walker, B., 2002.
782 Resilience and Sustainable Development: Building Adaptive Capacity in a World of
783 Transformations. AMBIO J. Hum. Environ. 31, 437–440.
784 https://doi.org/10.1579/0044-7447-31.5.437
785 Gil-García, C., Rigol, A., Vidal, M., 2009. New best estimates for radionuclide solid–liquid
786 distribution coefficients in soils, Part 1: radiostrontium and radiocaesium. J. Environ.
787 Radioact. 100, 690–696. https://doi.org/10.1016/j.jenvrad.2008.10.003
788 Grosbois, C., Meybeck, M., Horowitz, A., Ficht, A., 2006. The spatial and temporal trends of
789 Cd, Cu, Hg, Pb and Zn in Seine River floodplain deposits (1994–2000). Sci. Total
790 Environ. 356, 22–37. https://doi.org/10.1016/j.scitotenv.2005.01.049
791 Grygar, T.M., Elznicová, J., Kiss, T., Smith, H., 2016. Using sedimentary archives to
792 reconstruct pollution history and sediment provenance: the Ohře River, Czech
793 Republic. Catena 144, 109–129.
794 Gu, Z., Shi, C., Yang, H., Yao, H., 2019. Analysis of dynamic sedimentary environments in
795 alluvial fans of some tributaries of the upper Yellow River of China based on ground
796 penetrating radar (GPR) and sediment cores. Quat. Int., BRIDGING EUROPE AND
797 ASIA: QUATERNARY STRATIGRAPHY AND PALAEOLITHIC HUMAN
798 OCCUPATION 509, 30–40. https://doi.org/10.1016/j.quaint.2018.05.001

Guédron, S., Amouroux, D., Sabatier, P., Desplanque, C., Develle, A.-L., Barre, J., Feng, C., Guiter, F., Arnaud, F., Reyss, J.L., Charlet, L., 2016. A hundred year record of industrial and urban development in French Alps combining Hg accumulation rates and isotope composition in sediment archives from Lake Luitel. Chem. Geol. 431, 10–19. https://doi.org/10.1016/j.chemgeo.2016.03.016

Guermond, Y., 1981. Louviers - Le Vaudreuil : l'impact spatial d'un pôle d'emploi comme moyen d'évaluation du changement social. Norois 112, 577–598. https://doi.org/10.3406/noroi.1981.3996

Hanesch, M., Scholger, R., 2002. Mapping of heavy metal loadings in soils by means of magnetic susceptibility measurements. Environ. Geol. 42, 857–870. https://doi.org/10.1007/s00254-002-0604-1

Hatfield, R.G., Maher, B.A., 2009. Fingerprinting upland sediment sources: particle size-specific magnetic linkages between soils, lake sediments and suspended sediments. Earth Surf. Process. Landf. 34, 1359–1373. https://doi.org/10.1002/esp.1824

Hatfield, R.G., Maher, B.A., 2008. Suspended sediment characterization and tracing using a magnetic fingerprinting technique: Bassenthwaite Lake, Cumbria, UK. The Holocene 18, 105–115. https://doi.org/10.1177/0959683607085600

Hatfield, R.G., Stoner, J.S., 2013. Magnetic Proxies and Susceptibility. Elias SA Ed Encycl. Quat. Sci. 2, 884–898.

He, Q., Walling, D.E., 1996. Interpreting particle size effects in the adsorption of 137Cs and unsupported 210Pb by mineral soils and sediments. J. Environ. Radioact. 30, 117–137. https://doi.org/10.1016/0265-931X(96)89275-7

Hennekam, R., Sweere, T., Tjallingii, R., de Lange, G.J., Reichart, G.-J., 2019. Trace metal analysis of sediment cores using a novel X-ray fluorescence core scanning method. Quat. Int., Advances in Data Quantification and Application of high resolution XRF Core Scanners 514, 55–67. https://doi.org/10.1016/j.quaint.2018.10.018

Holling, C.S., 1973. Resilience and Stability of Ecological Systems. Annu. Rev. Ecol. Syst. 4, 1–23. https://doi.org/10.1146/annurev.es.04.110173.000245

Horowitz, A.J., Elrick, K.A., 1987. The relation of stream sediment surface area, grain size and composition to trace element chemistry. Appl. Geochem. 2, 437–451. https://doi.org/10.1016/0883-2927(87)90027-8

Horowitz, A.J., Elrick, K.A., Callender, E., 1988. The effect of mining on the sediment - trace element geochemistry of cores from the Cheyenne River arm of Lake Oahe, South Dakota, U.S.A. Chem. Geol. 67, 17–33. https://doi.org/10.1016/0009-2541(88)90003-4

Horowitz, A.J., Meybeck, M., Idlafkih, Z., Biger, E., 1999. Variations in trace element geochemistry in the Seine River Basin based on floodplain deposits and bed sediments. Hydrol. Process. 13, 1329–1340. https://doi.org/10.1002/(SICI)1099-1085(19990630)13:9<1329::AID-HYP811>3.0.CO;2-H

Huggenberger, P., Meier, E., Pugin, A., 1994. Ground-probing radar as a tool for heterogeneity estimation in gravel deposits: advances in data-processing and facies analysis. J. Appl. Geophys., Geophysics and Environment 31, 171–184. https://doi.org/10.1016/0926-9851(94)90056-6

Huggenberger, P., Regli, C., 2006. A Sedimentological Model to Characterize Braided River Deposits for Hydrogeological Applications, in: Sambrook Smith, G.H., Best, J.L., Bristow, C.S., Petts, G.E. (Eds.), Braided Rivers. Blackwell Publishing Ltd., Oxford, UK, pp. 51–74. https://doi.org/10.1002/9781444304374.ch3

IREP - Registre des Emissions Polluantes [WWW Document], n.d. URL http://www.georisques.gouv.fr/cartes-interactives#/show/http%3A%2F%2Fmapsref.brgm.fr%2Fwxs%2Fgeorisques%2Frisques%3Fid_query%3D9613/ETABLISSEMENTS_POLLUEURS_RECHERCHE/-

357823.2365,6037008.6939,1313632.3628,7230727.3772/EPSG:2154 (accessed 4.25.19).
James, L.A., 2018. Ten conceptual models of large-scale legacy sedimentation – A review. Geomorphology 317, 199–217. https://doi.org/10.1016/j.geomorph.2018.05.021
James, L.A., 2013. Legacy sediment: Definitions and processes of episodically produced anthropogenic sediment. Anthropocene, Geomorphology of the Anthropocene: Understanding The Surficial Legacy of Past and Present Human Activities 2, 16–26. https://doi.org/10.1016/j.ancene.2013.04.001
Kaci, A., Petit, F., Fournier, M., Cécillon, S., Boust, D., Lesueur, P., Berthe, T., 2016. Diversity of active microbial communities subjected to long-term exposure to chemical contaminants along a 40-year-old sediment core. Environ. Sci. Pollut. Res. 23, 4095–4110. https://doi.org/10.1007/s11356-015-4506-7
Kaci, A., Petit, F., Lesueur, P., Boust, D., Vrel, A., Berthe, T., 2014. Distinct diversity of the czcA gene in two sedimentary horizons from a contaminated estuarine core. Environ. Sci. Pollut. Res. 21, 10787–10802. https://doi.org/10.1007/s11356-014-3029-y
Knab, M., Hoffmann, V., Petrovský, E., Kapička, A., Jordanova, N., Appel, E., 2006. Surveying the anthropogenic impact of the Moldau river sediments and nearby soils using magnetic susceptibility. Environ. Geol. 49, 527–535. https://doi.org/10.1007/s00254-005-0080-5
Koiter, A.J., Owens, P.N., Petticrew, E.L., Lobb, D.A., 2013. The behavioural characteristics of sediment properties and their implications for sediment fingerprinting as an approach for identifying sediment sources in river basins. Earth-Sci. Rev. 125, 24–42. https://doi.org/10.1016/j.earscirev.2013.05.009
Kostic, B., Becht, A., Aigner, T., 2005. 3-D sedimentary architecture of a Quaternary gravel delta (SW-Germany): Implications for hydrostratigraphy. Sediment. Geol. 181, 147–171. https://doi.org/10.1016/j.sedgeo.2005.07.004
Krishnaswamy, S., Lal, D., Martin, J.M., Meybeck, M., 1971. Geochronology of lake sediments. Earth Planet. Sci. Lett. 11, 407–414. https://doi.org/10.1016/0012-821X(71)90202-0
Kurashige, Y., Fusejima, Y., 1997. Source identification of suspended sediment from grain-size distributions: I. Application of nonparametric statistical tests. CATENA 31, 39–52. https://doi.org/10.1016/S0341-8162(97)00033-7
Kylander, M.E., Ampel, L., Wohlfarth, B., Veres, D., 2011. High-resolution X-ray fluorescence core scanning analysis of Les Echets (France) sedimentary sequence: new insights from chemical proxies. J. Quat. Sci. 26, 109–117. https://doi.org/10.1002/jqs.1438
Laignel, B., Quesnel, F., Lecoustumer, M.-N., Meyer, R., 1998. Variabilité du cortège argileux des formations résiduelles à silex de l'Ouest du bassin de Paris. Comptes Rendus Académie Sci. - Ser. IIA - Earth Planet. Sci. 326, 467–472. https://doi.org/10.1016/S1251-8050(98)80072-4
Le Cloarec, M.-F., Bonte, P.H., Lestel, L., Lefèvre, I., Ayrault, S., 2011. Sedimentary record of metal contamination in the Seine River during the last century. Phys. Chem. Earth Parts ABC, Man and River Systems: From pressures to physical, chemical and ecological status 36, 515–529. https://doi.org/10.1016/j.pce.2009.02.003
Lepland, Aivo, Andersen, T.J., Lepland, Aave, Arp, H.P.H., Alve, E., Breedveld, G.D., Rindby, A., 2010. Sedimentation and chronology of heavy metal pollution in Oslo harbor, Norway. Mar. Pollut. Bull. 60, 1512–1522. https://doi.org/10.1016/j.marpolbul.2010.04.017
Lestel, L., Eschbach, D., Steinmann, R., Gastaldi, N., 2019. ArchiSEINE : une approche géohistorique du bassin de la Seine (No. 18).

Lewis, S.L., Maslin, M.A., 2015. Defining the Anthropocene. Nature 519, 171–180. https://doi.org/10.1038/nature14258
Lin, Y.-T., Schuettpelz, C.C., Wu, C.H., Fratta, D., 2009. A combined acoustic and electromagnetic wave-based techniques for bathymetry and subbottom profiling in shallow waters. J. Appl. Geophys. 68, 203–218. https://doi.org/10.1016/j.jappgeo.2008.11.010
Livens, F.R., Baxter, M.S., 1988. Particle size and radionuclide levels in some west Cumbrian soils. Sci. Total Environ., Environmental Radiochemical Analysis 70, 1–17. https://doi.org/10.1016/0048-9697(88)90248-3
Lorgeoux, C., Moilleron, R., Gasperi, J., Ayrault, S., Bonté, P., Lefèvre, I., Tassin, B., 2016. Temporal trends of persistent organic pollutants in dated sediment cores: Chemical fingerprinting of the anthropogenic impacts in the Seine River basin, Paris. Sci. Total Environ. 541, 1355–1363. https://doi.org/10.1016/j.scitotenv.2015.09.147
Mabit, L., Benmansour, M., Abril, J.M., Walling, D.E., Meusburger, K., Iurian, A.R., Bernard, C., Tarján, S., Owens, P.N., Blake, W.H., Alewell, C., 2014. Fallout 210Pb as a soil and sediment tracer in catchment sediment budget investigations: A review. Earth-Sci. Rev. 138, 335–351. https://doi.org/10.1016/j.earscirev.2014.06.007
Magiera, T., Strzyszcz, Z., Kapicka, A., Petrovsky, E., 2006. Discrimination of lithogenic and anthropogenic influences on topsoil magnetic susceptibility in Central Europe. Geoderma 130, 299–311. https://doi.org/10.1016/j.geoderma.2005.02.002
Masson, M., Blanc, G., Schäfer, J., 2006. Geochemical signals and source contributions to heavy metal (Cd, Zn, Pb, Cu) fluxes into the Gironde Estuary via its major tributaries. Sci. Total Environ. 370, 133–146. https://doi.org/10.1016/j.scitotenv.2006.06.011
Masson, M., Blanc, G., Schäfer, J., Parlanti, E., Le Coustumer, P., 2011. Copper addition by organic matter degradation in the freshwater reaches of a turbid estuary. Sci. Total Environ. 409, 1539–1549. https://doi.org/10.1016/j.scitotenv.2011.01.022
Mellett, J.S., 1995. Profiling of ponds and bogs using ground-penetrating radar. J. Paleolimnol. 14, 233–240. https://doi.org/10.1007/BF00682425
Meybeck, M., Lestel, L., Bonté, P., Moilleron, R., Colin, J.L., Rousselot, O., Hervé, D., de Pontevès, C., Grosbois, C., Thévenot, D.R., 2007. Historical perspective of heavy metals contamination (Cd, Cr, Cu, Hg, Pb, Zn) in the Seine River basin (France) following a DPSIR approach (1950–2005). Sci. Total Environ., Human activity and material fluxes in a regional river basin: the Seine River watershed 375, 204–231. https://doi.org/10.1016/j.scitotenv.2006.12.017
Monna, F., Lancelot, J., Bernat, M., Mercadier, H., 1998. Sedimentation rate in the Thau basin (France) according to geochronological, geochemical and stratigraphical data. Oceanogr. Lit. Rev. 2, 279–280.
Müller, J., Ruppert, H., Muramatsu, Y., Schneider, J., 2000. Reservoir sediments – a witness of mining and industrial development (Malter Reservoir, eastern Erzgebirge, Germany). Environ. Geol. 39, 1341–1351. https://doi.org/10.1007/s002540000117
Neal, A., 2004. Ground-penetrating radar and its use in sedimentology: principles, problems and progress. Earth-Sci. Rev. 66, 261–330. https://doi.org/10.1016/j.earscirev.2004.01.004
Nguyen, H.L., Braun, M., Szaloki, I., Baeyens, W., Van Grieken, R., Leermakers, M., 2009. Tracing the Metal Pollution History of the Tisza River Through the Analysis of a Sediment Depth Profile. Water. Air. Soil Pollut. 200, 119–132. https://doi.org/10.1007/s11270-008-9898-2
Nilsson, C., Reidy, C.A., Dynesius, M., Revenga, C., 2005. Fragmentation and Flow Regulation of the World's Large River Systems. Science 308, 405–408. https://doi.org/10.1126/science.1107887

O'Driscoll, M., Johnson, P., Mallinson, D., 2010. Geological controls and effects of floodplain asymmetry on river–groundwater interactions in the southeastern Coastal Plain, USA. Hydrogeol. J. 18, 1265–1279. https://doi.org/10.1007/s10040-010-0595-z

Petit, J.C.J., Schäfer, J., Coynel, A., Blanc, G., Deycard, V.N., Derriennic, H., Lanceleur, L., Dutruch, L., Bossy, C., Mattielli, N., 2013. Anthropogenic sources and biogeochemical reactivity of particulate and dissolved Cu isotopes in the turbidity gradient of the Garonne River (France). Chem. Geol. 359, 125–135. https://doi.org/10.1016/j.chemgeo.2013.09.019

Pittam, N.J., Foster, I.D.L., Mighall, T.M., 2009. An integrated lake-catchment approach for determining sediment source changes at Aqualate Mere, Central England. J. Paleolimnol. 42, 215–232. https://doi.org/10.1007/s10933-008-9272-9

Pulley, S., Van der Waal, B., Rowntree, K., Collins, A.L., 2018. Colour as reliable tracer to identify the sources of historically deposited flood bench sediment in the Transkei, South Africa: A comparison with mineral magnetic tracers before and after hydrogen peroxide pre-treatment. CATENA 160, 242–251. https://doi.org/10.1016/j.catena.2017.09.018

Quesnel, F., 1997. Digital mapping in regolith geology. Cartographie numérique en géologie de surface. Application aux altérites à silex de l'Ouest du bassin de Paris (Theses). Université de Rouen.

Richter, T.O., Gaast, S. van der, Koster, B., Vaars, A., Gieles, R., Stigter, H.C. de, Haas, H.D., Weering, T.C.E. van, 2006. The Avaatech XRF Core Scanner: technical description and applications to NE Atlantic sediments. Geol. Soc. Lond. Spec. Publ. 267, 39–50. https://doi.org/10.1144/GSL.SP.2006.267.01.03

Robbins, J.A., Edgington, D.N., 1975. Determination of recent sedimentation rates in Lake Michigan using Pb-210 and Cs-137. Geochim. Cosmochim. Acta 39, 285–304. https://doi.org/10.1016/0016-7037(75)90198-2

Sabatier, P., Poulenard, J., Fanget, B., Reyss, J.-L., Develle, A.-L., Wilhelm, B., Ployon, E., Pignol, C., Naffrechoux, E., Dorioz, J.-M., Montuelle, B., Arnaud, F., 2014. Long-term relationships among pesticide applications, mobility, and soil erosion in a vineyard watershed. Proc. Natl. Acad. Sci. U. S. A. 111, 15647–15652. https://doi.org/10.1073/pnas.1411512111

Sebag, D., Debret, M., M'voubou, M., Obame, R.M., Ngomanda, A., Oslisly, R., Bentaleb, I., Disnar, J.-R., Giresse, P., 2013. Coupled Rock-Eval pyrolysis and spectrophotometry for lacustrine sedimentary dynamics: Application for West Central African rainforests (Kamalété and Nguène lakes, Gabon). The Holocene 23, 1173–1183. https://doi.org/10.1177/0959683613483622

Sebok, E., Karan, S., Engesgaard, P., 2018. Using hydrogeophysical methods to assess the feasibility of lake bank filtration. J. Hydrol. 562, 423–434. https://doi.org/10.1016/j.jhydrol.2018.04.049

Shuman, J.R., 1995. Environmental considerations for assessing dam removal alternatives for river restoration. Regul. Rivers Res. Manag. 11, 249–261. https://doi.org/10.1002/rrr.3450110302

Singh, N., Li, J., Zeng, X., 2016. Solutions and challenges in recycling waste cathode-ray tubes. J. Clean. Prod. 133, 188–200. https://doi.org/10.1016/j.jclepro.2016.04.132

Słowik, M., 2015. Is history of rivers important in restoration projects? The example of human impact on a lowland river valley (the Obra River, Poland). Geomorphology, Emerging geomorphic approaches to guide river management practices 251, 50–63. https://doi.org/10.1016/j.geomorph.2015.05.031

Stanley, E.H., Doyle, M.W., 2003. Trading off: the ecological effects of dam removal. Front. Ecol. Environ. 1, 15–22. https://doi.org/10.1890/1540-9295(2003)001[0015:TOTEEO]2.0.CO;2

Steffen, W., Grinevald, J., Crutzen, P., McNeill, J., 2011. The Anthropocene: conceptual and historical perspectives. Philos. Trans. R. Soc. Math. Phys. Eng. Sci. 369, 842–867. https://doi.org/10.1098/rsta.2010.0327

Tamtam, F., Le Bot, B., Dinh, T., Mompelat, S., Eurin, J., Chevreuil, M., Bonté, P., Mouchel, J.-M., Ayrault, S., 2011. A 50-year record of quinolone and sulphonamide antimicrobial agents in Seine River sediments. J. Soils Sediments 11, 852–859. https://doi.org/10.1007/s11368-011-0364-1

Thibert, S., 1994. Exportations naturelles et anthropiques des ions majeurs et des éléments nutritifs dans le bassin de la Seine : approches méthodologiques. Université Pierre et Marie Curie - Paris VI.

Tissot, B.P., Welte, D.H., 1984. Petroleum Formation and Occurrence, 2nd edition. ed. Springer, Heidelberg.

Toonen, W.H.J., Winkels, T.G., Cohen, K.M., Prins, M.A., Middelkoop, H., 2015. Lower Rhine historical flood magnitudes of the last 450years reproduced from grain-size measurements of flood deposits using End Member Modelling. CATENA, Past Hydrological Extreme Events in a Changing Climate 130, 69–81. https://doi.org/10.1016/j.catena.2014.12.004

Tseng, C.M., Amouroux, D., Abril, G., Tessier, E., Etcheber, H., Donard, O.F.X., 2001. Speciation of Mercury in a Fluid Mud Profile of a Highly Turbid Macrotidal Estuary (Gironde, France). Environ. Sci. Technol. 35, 2627–2633. https://doi.org/10.1021/es001750b

Tsydenova, O., Bengtsson, M., 2011. Chemical hazards associated with treatment of waste electrical and electronic equipment. Waste Manag. 31, 45–58. https://doi.org/10.1016/j.wasman.2010.08.014

Van Metre, P.C., Callender, E., Fuller, C.C., 1997. Historical Trends in Organochlorine Compounds in River Basins Identified Using Sediment Cores from Reservoirs. Environ. Sci. Technol. 31, 2339–2344. https://doi.org/10.1021/es960943p

Van Metre, P.C., Mesnage, V., Laignel, B., Motelay, A., Deloffre, J., 2008. Origins of Sediment-Associated Contaminants to the Marais Vernier, the Seine Estuary, France. Water. Air. Soil Pollut. 191, 331–344. https://doi.org/10.1007/s11270-008-9628-9

Vrel, A., 2012. Reconstitution de l'historique des apports en radionucléides et contaminants métalliques à l'estuaire fluvial de la Seine par l'analyse de leur enregistrement sédimentaire.

Vrel, A., Boust, D., Lesueur, P., Deloffre, J., Dubrulle-Brunaud, C., Solier, L., Rozet, M., Thouroude, C., Cossonnet, C., Thomas, S., 2013. Dating of sediment record at two contrasting sites of the Seine River using radioactivity data and hydrological time series. J. Environ. Radioact. 126, 20–31. https://doi.org/10.1016/j.jenvrad.2013.06.005

Walling, D.E., Owens, P.N., Carter, J., Leeks, G.J.L., Lewis, S., Meharg, A.A., Wright, J., 2003. Storage of sediment-associated nutrients and contaminants in river channel and floodplain systems. Appl. Geochem. 18, 195–220. https://doi.org/10.1016/S0883-2927(02)00121-X

Walling, D.E., Woodward, J.C., 1992. Use of radiometric fingerprints to derive information on suspended sediment sources. Eros. Sediment Transp. Monit. Programme River Basins 153–64.

Wang, K., Cornett, R.J., 1993. Distribution coefficients of210Pb and210Po in laboratory and natural aquatic systems. J. Paleolimnol. 9, 179–188. https://doi.org/10.1007/BF00677519

Weltje, G.J., 2012. Quantitative models of sediment generation and provenance: State of the art and future developments. Sediment. Geol., Actualistic Models of Sediment Generation 280, 4–20. https://doi.org/10.1016/j.sedgeo.2012.03.010

Winkels, H.J., Kroonenberg, S.B., Lychagin, M.Y., Marin, G., Rusakov, G.V., Kasimov, N.S., 1998. Geochronology of priority pollutants in sedimentation zones of the Volga and Danube delta in comparison with the Rhine delta. Appl. Geochem. 13, 581–591. https://doi.org/10.1016/S0883-2927(98)00002-X

Yang, Z., Wang, H., Saito, Y., Milliman, J.D., Xu, K., Qiao, S., Shi, G., 2006. Dam impacts on the Changjiang (Yangtze) River sediment discharge to the sea: The past 55 years and after the Three Gorges Dam. Water Resour. Res. 42. https://doi.org/10.1029/2005WR003970

Figure 1. A. Historic sediment core sites in the lower reaches of the Seine River watershed and sediment core sites in the Eure River (present study). The length, time period represented and chemicals elements studied for each core sites are also mentioned; B. The Eure River watershed (present study). The Yonne and Oise rivers sub-watersheds studied in Ayrault et al., 2010b and Le Cloarec et al., 2011 are also represented.

Figure 2. Morphological modifications of Martot Pond and Les Damps Pond study sites established from several unpublished documents (e.g. maps from "Pont et Chaussées" and meeting minutes) stored at "Voie Navigable de France" (VNF). The cities of Martot, Pont-de-l'Arche et Les Damps have been indicated on the maps to facilitate comparison with the actual study area.

Figure 3. A. Study Area; B. Sediment core and GPR profiles locations in Les Damps Pond; C. Sediment core and GPR profiles locations in Martot Pond.

Figure 4. A1. Colour log; and B. Grain size distribution and D_{50}; A2. Colour log; C. TOC, HI, and OI; D. Magnetic susceptibility (MS) and reflectance (L*); E. First derivative values; F. Pb/Ti, Zn/Ti, Cu/Ti, and Ni/Ti ratios along the DAM15-02 and DAM17-02 cores collected in Les Damps Pond.

Figure 5. A. Colour log; B. Grain size distribution and D50; C. TOC, HI, and OI; D. Magnetic susceptibility (MS) and reflectance (L*); E. First derivative values; F. Pb/Ti, Zn/Ti, Cu/Ti and Ni/Ti ratios along MAR15-01 core collected in Martot Pond.

Figure 6. Pb/Ti, Zn/Ti, and Cu/Ti ratios along the upper part of the MAR16-02 core. Pb (dark circle), Zn (dark square) and Cu (dark triangle) concentrations are also presented.

Figure 7. A. $^{210}Pb_{ex}$; B. ^{137}Cs and. ^{241}Am; C. Age model for the MAR15-01 core.

Figure 8. Radargram performed with a 400 mHz antenna, migration rate used: 0.075 m ns^{-1}. Due to the lengths and depths reached and to obtain adequate readability, the x-scales of the 3 profiles are different. For reasons of navigability, all the core sampling points previously presented could not be documented by GPR, in particular the MAR15-01 and DAM15-02 cores A. GPR-MAR_08 radargram, processed and interpreted from Martot Pond. To obtain a 2D information, the MAR15-02, MAR15-03, MAR15-04, and MAR15-06 cores with a simple description distinguishing only the U1 and U2 facies, have been positioned; B. GPR_DAM_03 radargram processed and interpreted from Les Damps Pond. The DAM15-03 and DAM18-02 cores have been positioned; C. GRP_DAM_05 radargram, processed and interpreted from Les Damps Pond. The DAM17-02 core has been positioned.

Figure 9. A. Pseudo Van-Krevelen diagram; B. Q7/4 vs L* ratio for the MAR15-01 core (U1 and U2 facies) and the DAM17-02 core.

Figure 10. Evolution of Pb/Ti, Zn/Ti, Cu/Ti, and Ni/Ti ratios along the Eure Unit (MAR15-01 core).

Figure S11. Correlation matrix with XRF core scanning data (Al, Si, Fe, Ti, Mn, Zn, Cu, Ni, and Pb), TOC, and grain size (D_{50}, clay (< 2 µm), silt (2-63 µm), and coarse fraction (> 63 µm)) from the Eure Unit of the MAR15-01 core (Pearson correlation, p-value < 0.001 for all the R < -0.6 and R > 0.6).

Tableau 1. Characteristics of sediment cores collected in Les Damps Pond and Martot Pond (WGS 84).

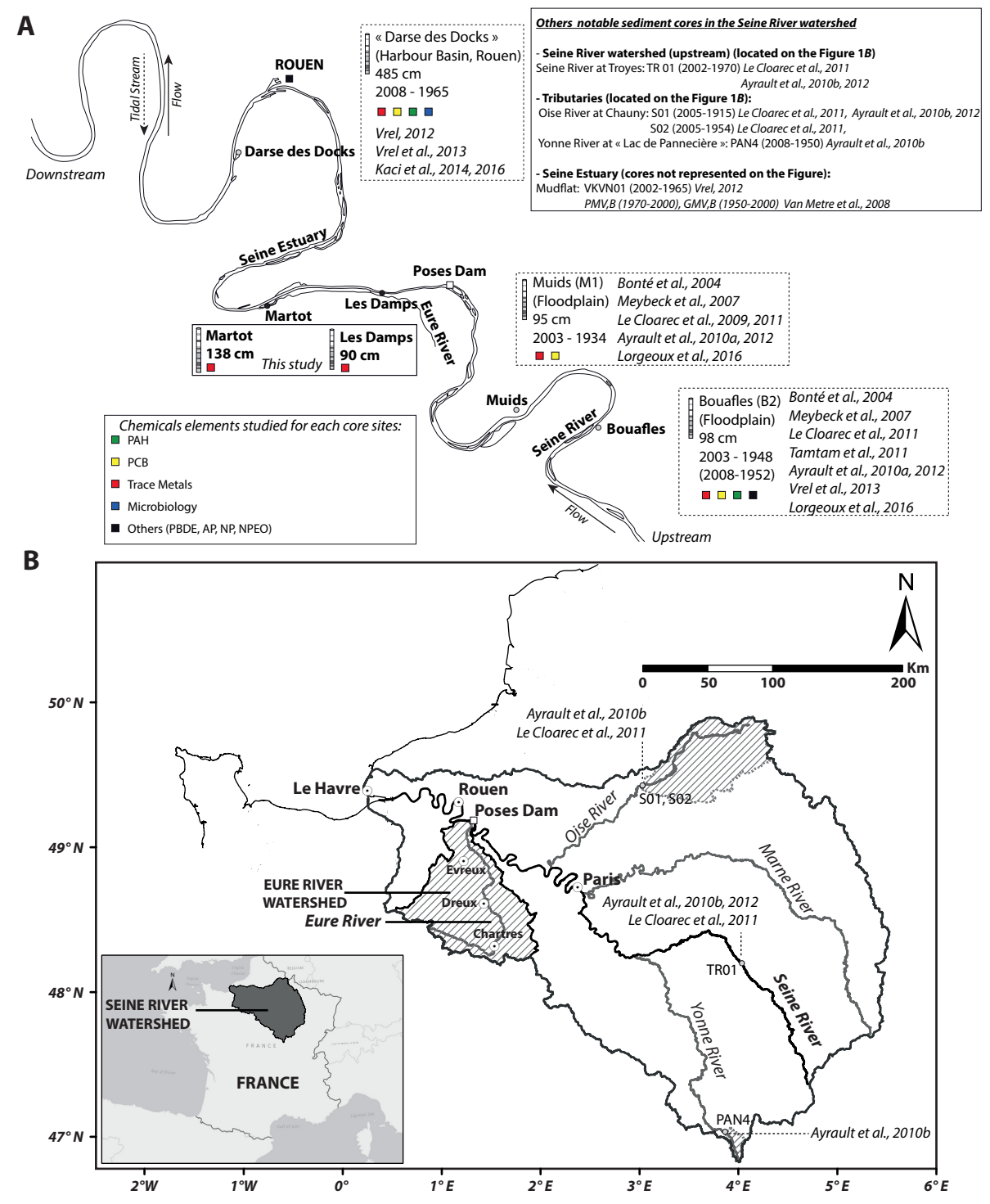
A
ROUEN
Tidal Stream
Flow
Downstream
Darse des Docks
« Darse des Docks »
(Harbour Basin, Rouen)
485 cm
2008 - 1965
Vrel, 2012
Vrel et al., 2013
Kaci et al., 2014, 2016
Others notable sediment cores in the Seine River watershed
- Seine River watershed (upstream) (located on the Figure 1B)
Seine River at Troyes: TR 01 (2002-1970) Le Cloarec et al., 2011
Ayrault et al., 2010b, 2012
- Tributaries (located on the Figure 1B):
Oise River at Chauny: S01 (2005-1915) Le Cloarec et al., 2011, Ayrault et al., 2010b, 2012
S02 (2005-1954) Le Cloarec et al., 2011,
Yonne River at « Lac de Pannecière »: PAN4 (2008-1950) Ayrault et al., 2010b
- Seine Estuary (cores not represented on the Figure):
Mudflat: VKVN01 (2002-1965) Vrel, 2012
PMV,B (1970-2000), GMV,B (1950-2000) Van Metre et al., 2008
Seine Estuary
Poses Dam
Les Damps
Martot
Martot
138 cm
This study
Les Damps
90 cm
Eure River
Muids (M1)
(Floodplain)
95 cm
2003 - 1934
Bonté et al., 2004
Meybeck et al., 2007
Le Cloarec et al., 2009, 2011
Ayrault et al., 2010a, 2012
Lorgeoux et al., 2016
Muids
Seine River
Bouafles
Bouafles (B2)
(Floodplain)
98 cm
2003 - 1948
(2008-1952)
Bonté et al., 2004
Meybeck et al., 2007
Le Cloarec et al., 2011
Tamtam et al., 2011
Ayrault et al., 2010a, 2012
Vrel et al., 2013
Lorgeoux et al., 2016
Chemicals elements studied for each core sites:
PAH
PCB
Trace Metals
Microbiology
Others (PBDE, AP, NP, NPEO)
Flow
Upstream
B
N
0
50
100
200
Km
50° N
49° N
48° N
47° N
2°W
1°W
0°
1° E
2° E
3° E
4° E
5° E
6° E
Ayrault et al., 2010b
Le Cloarec et al., 2011
Le Havre
Rouen
Poses Dam
S01, S02
Oise River
Paris
Marne River
Evreux
EURE RIVER
WATERSHED
Eure River
Dreux
Chartres
Ayrault et al., 2010b, 2012
Le Cloarec et al., 2011
TR01
Seine River
Yonne River
PAN4
Ayrault et al., 2010b
SEINE RIVER
WATERSHED
FRANCE

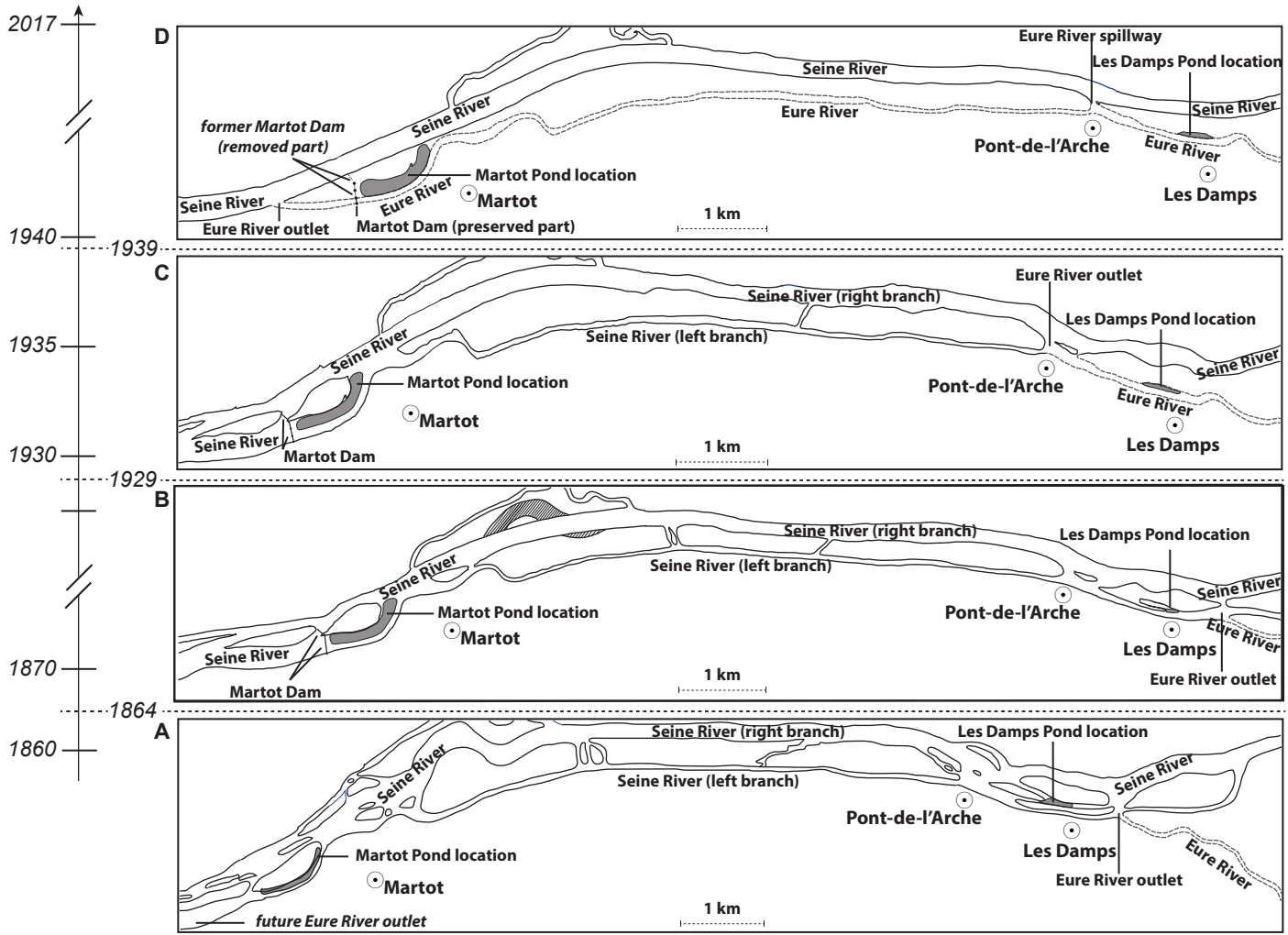
2017
1940
1939
1935
1930
1929
1870
1864
1860
D
Eure River spillway
Les Damps Pond location
Seine River
Eure River
Seine River
former Martot Dam
(removed part)
Seine River
Seine River
Pont-de-l'Arche
Eure River
Martot Pond location
Martot
Les Damps
Seine River
Eure River outlet
Eure River
Martot Dam (preserved part)
1 km
C
Eure River outlet
Seine River (right branch)
Les Damps Pond location
Seine River
Seine River (left branch)
Seine River
Martot Pond location
Pont-de-l'Arche
Martot
Eure River
Seine River
Les Damps
Martot Dam
1 km
B
Seine River (right branch)
Les Damps Pond location
Seine River
Seine River (left branch)
Seine River
Martot Pond location
Pont-de-l'Arche
Martot
Les Damps
Eure River
Seine River
Eure River outlet
Martot Dam
1 km
A
Seine River (right branch)
Les Damps Pond location
Seine River
Seine River (left branch)
Seine River
Pont-de-l'Arche
Martot Pond location
Les Damps
Eure River
Martot
Eure River outlet
future Eure River outlet
1 km

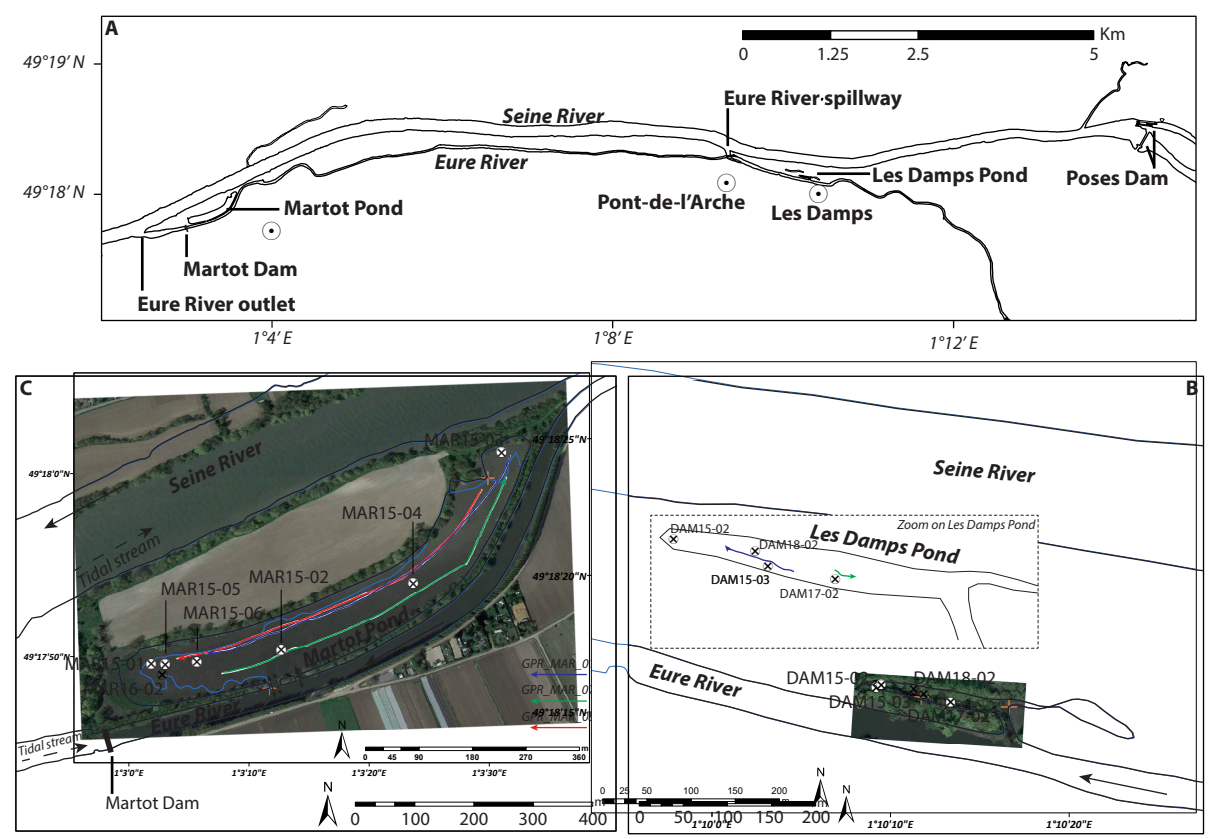
A
Km
0
1.25
2.5
5
49°19′N
49°18′N
Seine River
Eure River
Eure River·spillway
Les Damps Pond
Poses Dam
Pont-de-l'Arche
Les Damps
Martot Pond
Martot Dam
Eure River outlet
1°4′E
1°8′E
1°12′E
C
B
Seine River
Tidal stream
MAR15-01
MAR15-04
MAR15-05
MAR15-02
MAR15-06
MAR15-03
MAR16-01
Martot Pond
Eure River
GPR_MAR_0
GPR_MAR_0
GPR_MAR_0
49°18'15"N
49°18'0"N
49°18'20"N
49°17'50"N
1°3'0"E
1°3'10"E
1°3'20"E
1°3'30"E
Martot Dam
0
45
90
180
270
360
m
0
100
200
300
400
Zoom on Les Damps Pond
DAM15-02
DAM18-02
DAM15-03
DAM17-02
Les Damps Pond
Eure River
DAM15-01
DAM18-02
DAM15-03
DAM17-02
0
25
50
100
150
200
m
0
50
100
150
200
1°10'0"E
1°10'10"E
1°10'20"E

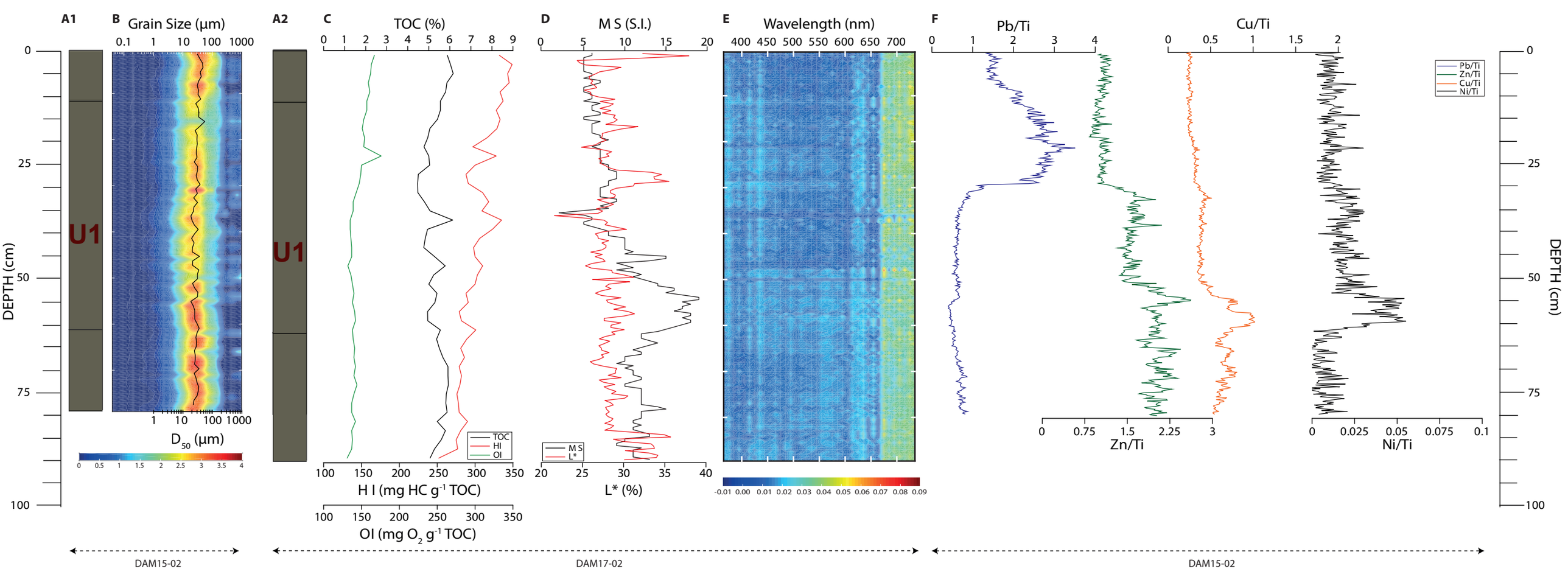
A1
B
Grain Size (μm)
0.1 1 10 100 1000
A2
C
TOC (%)
0 1 2 3 4 5 6 7 8 9
D
M S (S.I.)
0 5 10 15 20
E
Wavelength (nm)
400 450 500 550 600 650 700
F
Pb/Ti
0 1 2 3 4
Cu/Ti
0 0.5 1 1.5 2
U1
U1
DEPTH (cm)
0 25 50 75 100
1 10 100 1000
D50 (μm)
0 0.5 1 1.5 2 2.5 3 3.5 4
TOC
HI
OI
100 150 200 250 300 350
HI (mg HC g-1 TOC)
100 150 200 250 300 350
OI (mg O2 g-1 TOC)
MS
L*
20 25 30 35 40
L* (%)
-0.01 0.00 0.01 0.02 0.03 0.04 0.05 0.06 0.07 0.08 0.09
Pb/Ti
Zn/Ti
Cu/Ti
Ni/Ti
0 0.75 1.5 2.25 3
Zn/Ti
0 0.025 0.05 0.075 0.1
Ni/Ti
DAM15-02
DAM17-02
DAM15-02

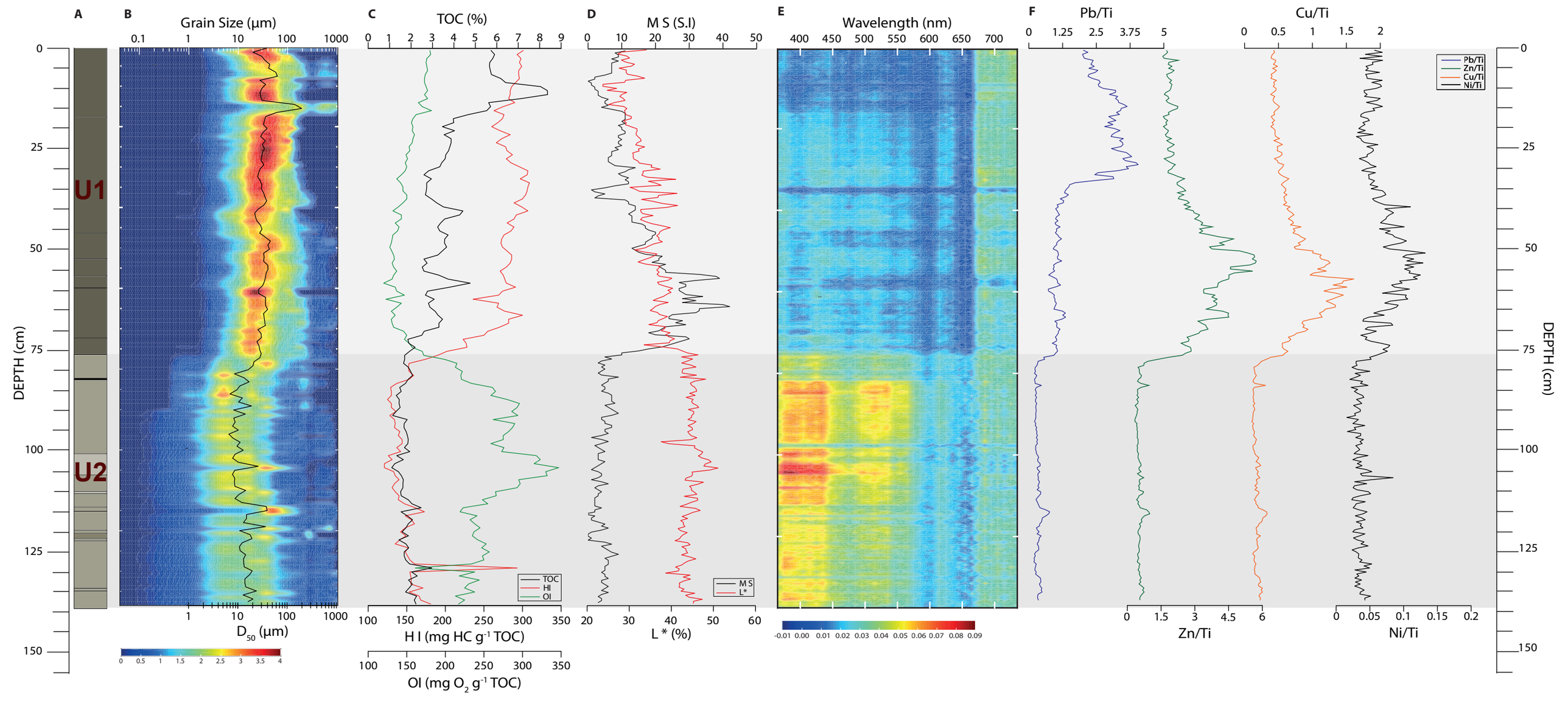
A
B
Grain Size (µm)
0.1
1
10
100
1000
C
TOC (%)
0
1
2
3
4
5
6
7
8
9
D
M S (S.I)
0
10
20
30
40
50
E
Wavelength (nm)
400
450
500
550
600
650
700
F
Pb/Ti
0
1.25
2.5
3.75
5
Cu/Ti
0
0.5
1
1.5
2
U1
U2
DEPTH (cm)
0
25
50
75
100
125
150
D50 (µm)
1
10
100
1000
0
0.5
1
1.5
2
2.5
3
3.5
4
TOC
HI
OI
100
150
200
250
300
350
H I (mg HC g-1 TOC)
OI (mg O2 g-1 TOC)
M S
L*
20
30
40
50
60
L * (%)
-0.01
0.00
0.01
0.02
0.03
0.04
0.05
0.06
0.07
0.08
0.09
Pb/Ti
Zn/Ti
Cu/Ti
Ni/Ti
0
1.5
3
4.5
6
Zn/Ti
0
0.05
0.1
0.15
0.2
Ni/Ti

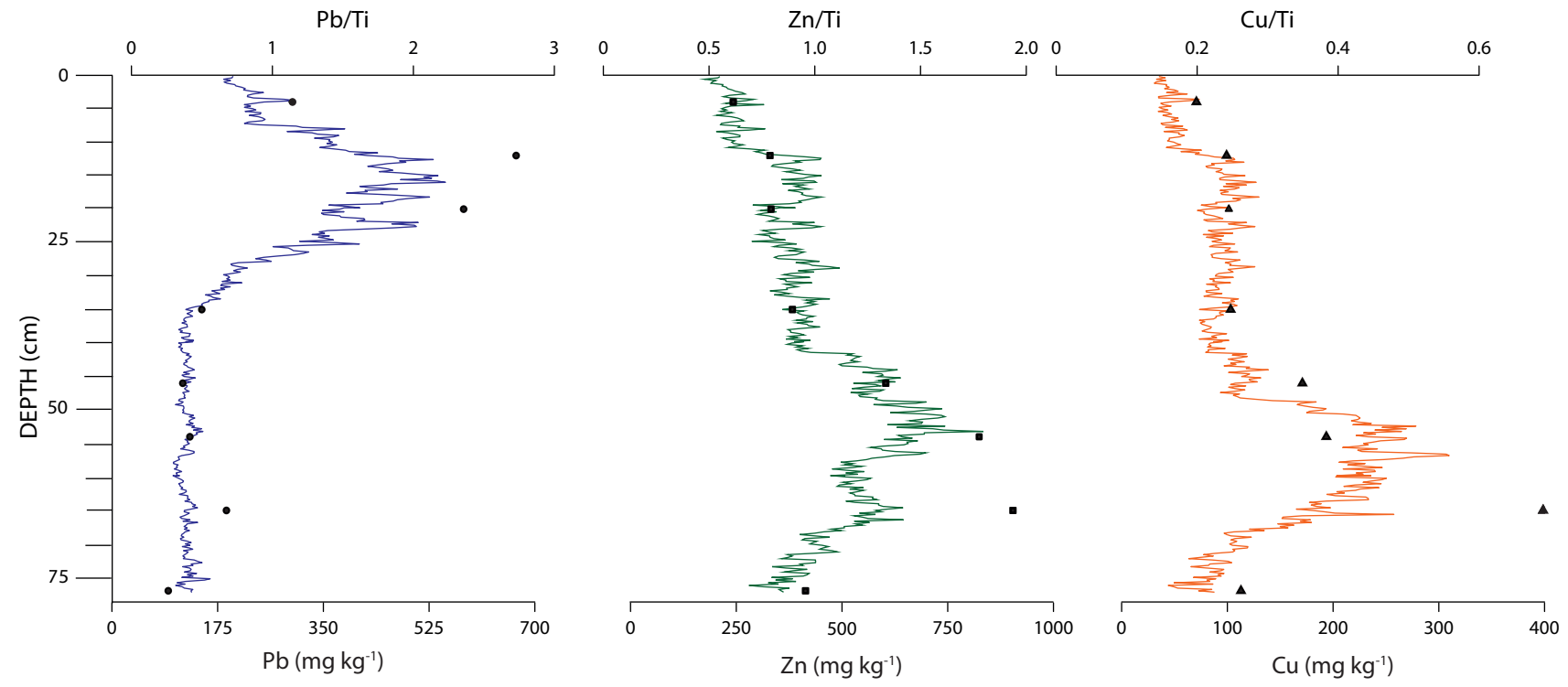
Pb/Ti
0
1
2
3
Zn/Ti
0
0.5
1.0
1.5
2.0
Cu/Ti
0
0.2
0.4
0.6
DEPTH (cm)
0
25
50
75
0
175
350
525
700
Pb (mg kg-1)
0
250
500
750
1000
Zn (mg kg-1)
0
100
200
300
400
Cu (mg kg-1)

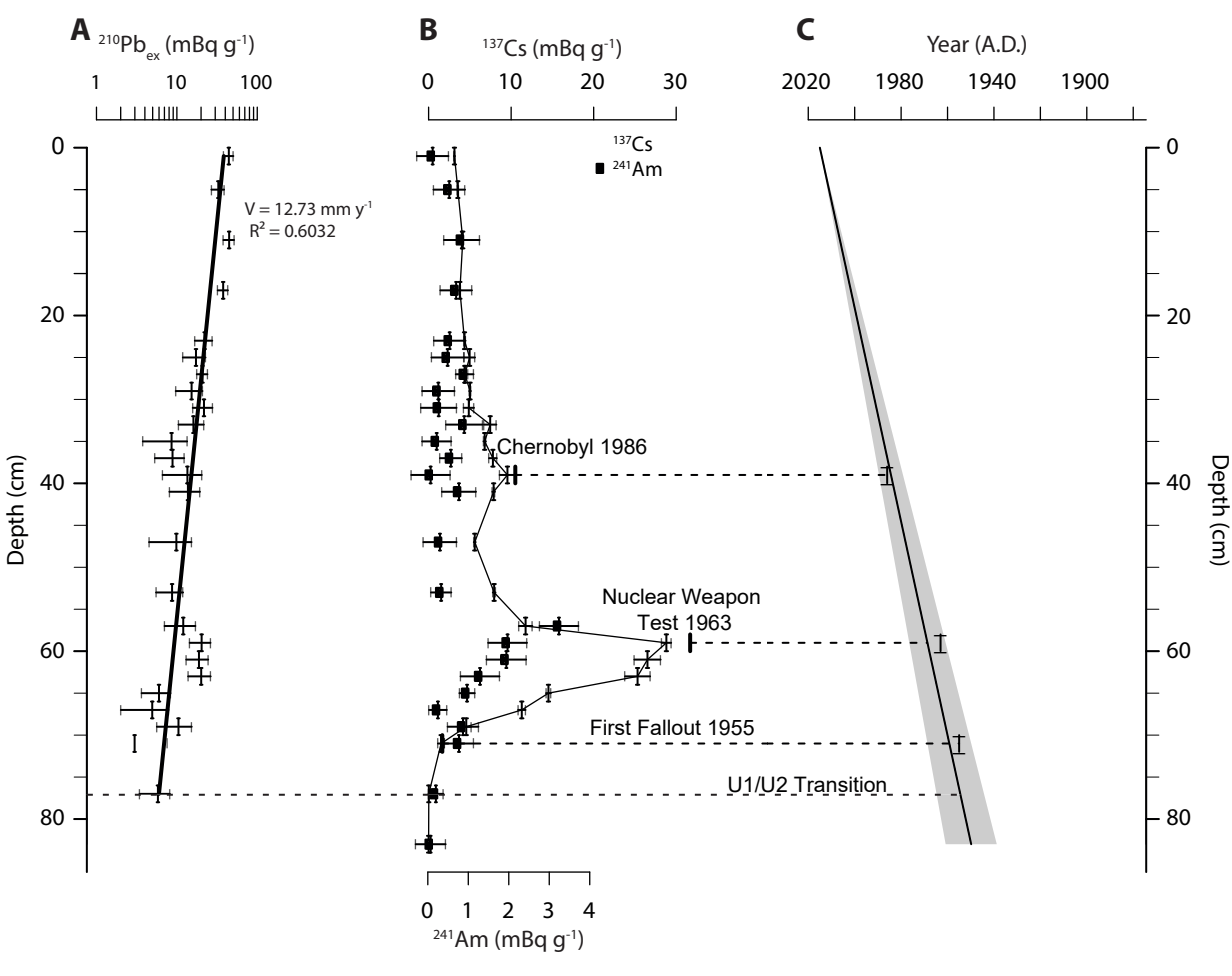
A
$^{210}Pb_{ex}$ (mBq g^{-1})
1
10
100
V = 12.73 mm y^{-1}
R^2 = 0.6032
B
^{137}Cs (mBq g^{-1})
0
10
20
30
^{137}Cs
^{241}Am
Chernobyl 1986
Nuclear Weapon
Test 1963
First Fallout 1955
U1/U2 Transition
0
1
2
3
4
^{241}Am (mBq g^{-1})
C
Year (A.D.)
2020
1980
1940
1900
Depth (cm)
0
20
40
60
80

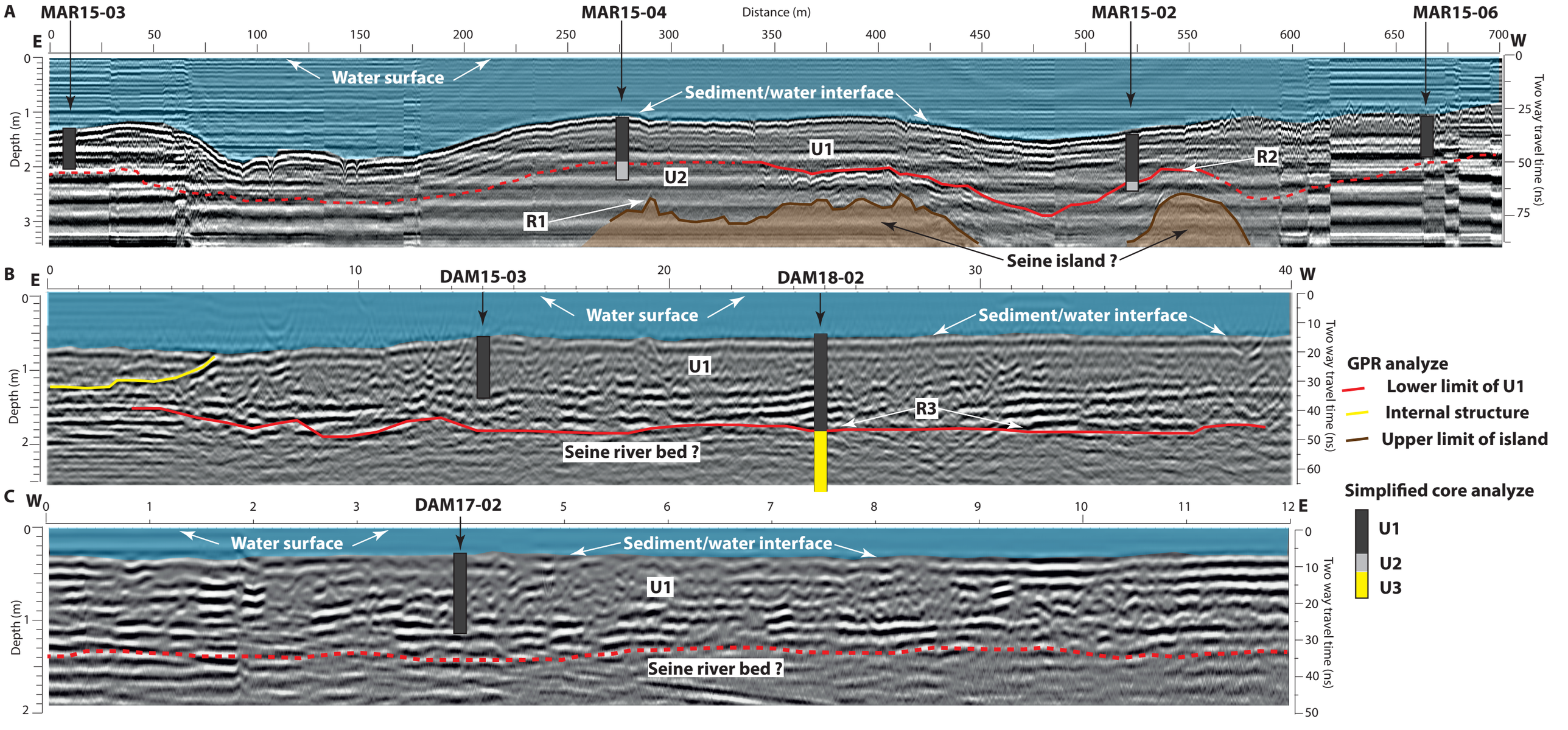
A
MAR15-03
MAR15-04
MAR15-02
MAR15-06
Distance (m)
E
W
Water surface
Sediment/water interface
U1
U2
R1
R2
Seine island ?
Depth (m)
Two way travel time (ns)
B
DAM15-03
DAM18-02
Water surface
Sediment/water interface
U1
R3
Seine river bed ?
C
DAM17-02
Water surface
Sediment/water interface
U1
Seine river bed ?
GPR analyze
Lower limit of U1
Internal structure
Upper limit of island
Simplified core analyze
U1
U2
U3

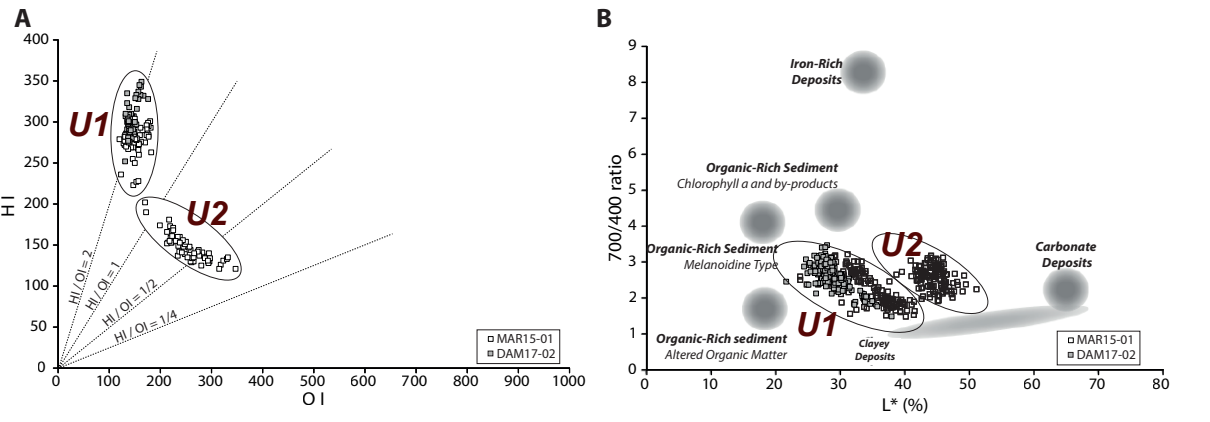
A
HI
OI
U1
U2
HI / OI = 2
HI / OI = 1
HI / OI = 1/2
HI / OI = 1/4
MAR15-01
DAM17-02
B
700/400 ratio
L* (%)
Iron-Rich Deposits
Organic-Rich Sediment
Chlorophyll a and by-products
Organic-Rich Sediment
Melanoidine Type
Organic-Rich sediment
Altered Organic Matter
Clayey Deposits
Carbonate Deposits
U1
U2
MAR15-01
DAM17-02

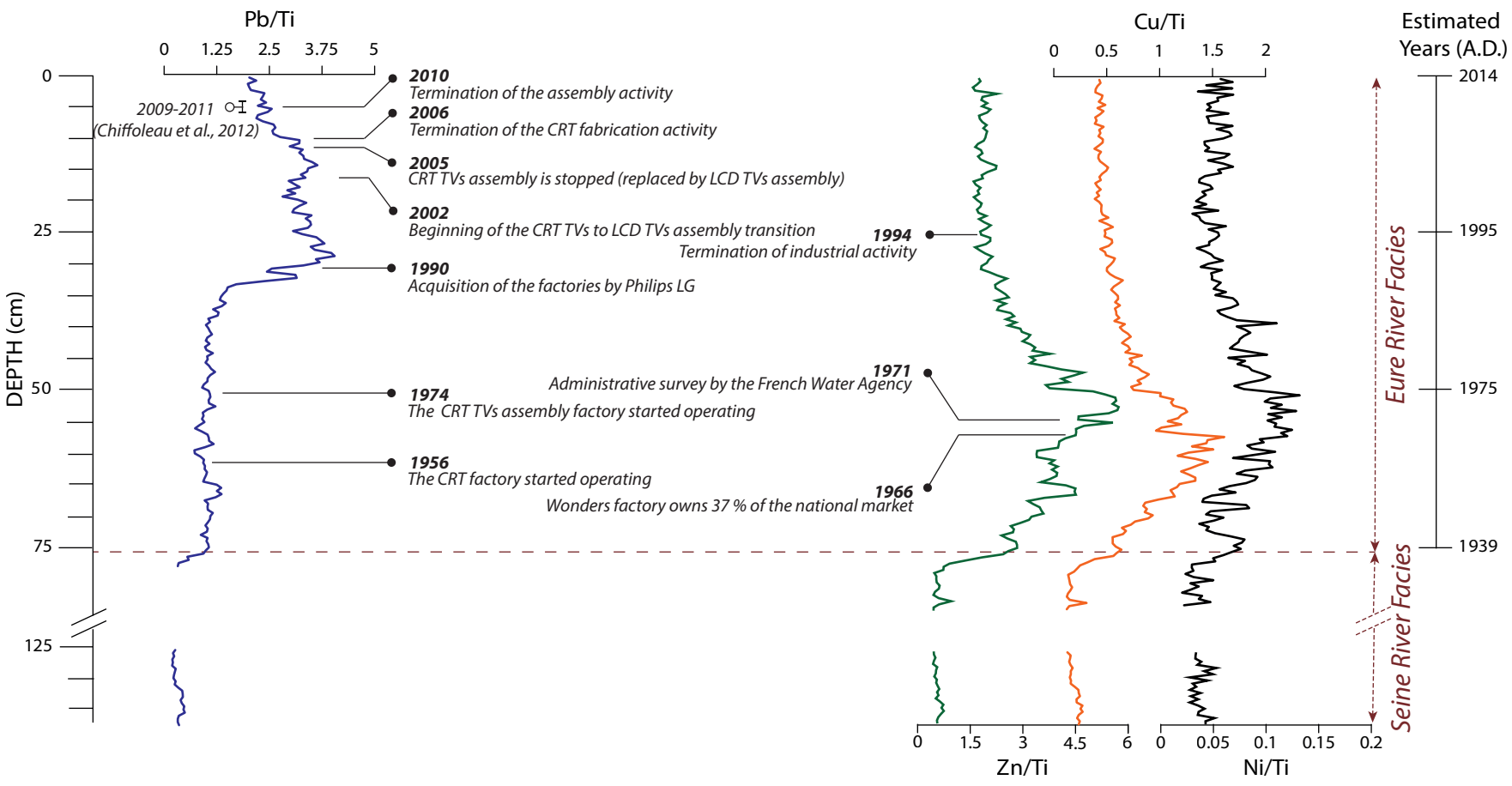
Pb/Ti
0
1.25
2.5
3.75
5
DEPTH (cm)
0
25
50
75
125
2009-2011
(Chiffoleau et al., 2012)
2010
Termination of the assembly activity
2006
Termination of the CRT fabrication activity
2005
CRT TVs assembly is stopped (replaced by LCD TVs assembly)
2002
Beginning of the CRT TVs to LCD TVs assembly transition
1990
Acquisition of the factories by Philips LG
1974
The CRT TVs assembly factory started operating
1956
The CRT factory started operating
Cu/Ti
0
0.5
1
1.5
2
1994
Termination of industrial activity
1971
Administrative survey by the French Water Agency
1966
Wonders factory owns 37 % of the national market
Zn/Ti
0
1.5
3
4.5
6
Ni/Ti
0
0.05
0.1
0.15
0.2
Estimated
Years (A.D.)
2014
1995
1975
1939
Eure River Facies
Seine River Facies

Pond	Core ID	IGSN	Longitude (X)	Latitude (Y)	Core Length (cm)
LES DAMPS (DAM)	DAM15-02	IEM2C0016	1°10'9.05" E	49°18'16.13" N	80
	DAM15-03	IEM2C0017	1°10'11.58" E	49°18'15.83" N	67
	DAM17-02	IEM2C000E	1°10'13.26" E	49°18'15.66" N	90
	DAM18-02	IEM2C001C	1°10’11.14" E	49°18’16.09" N	208
MARTOT (MAR)	MAR15-01	IEM2C0001	1°03'1.68" E	49°17'49.68" N	138
	MAR15-02	IEM2C0002	1°03'12.49" E	49°17'50.63" N	93
	MAR15-03	IEM2C0003	1°03'30.45" E	49°18'1.69" N	68
	MAR15-04	IEM2C0004	1°03'23.34" E	49°17'54.44" N	104
	MAR15-05	IEM2C0005	1°03'2.84" E	49°17'49.69" N	161
	MAR15-06	IEM2C0006	1°03'5.49" E	49°17'49.88" N	96
	MAR16-02	IEM2C0008	1°03'2.60" E	49°17'49.30" N	129